



OPEN ACCESS

EDITED BY
Ali Abedini,
Urmia University, Iran

REVIEWED BY
Sara Dargahi,
Shahid Bahonar University of
Kerman, Iran
Masoumeh Ahangari,
Urmia University, Iran

*CORRESPONDENCE
Jinyan Lin,
geo-s209@163.com
Yuanyuan Xiao,
yuanyuan.xiao@qdio.ac.cn

SPECIALTY SECTION
This article was submitted to
Geochemistry,
a section of the journal
Frontiers in Earth Science

RECEIVED 24 July 2022
ACCEPTED 31 October 2022
PUBLISHED 12 January 2023

CITATION
Kong J, Wang L, Yao Y, Lin J, Xiao Y and
Yang Y (2023), Petrology and
geochemical characteristics of
amphibolite facies rocks in Xunyangba
area, South Qinling Orogen,
Central China.
Front. Earth Sci. 10:1001795.
doi: 10.3389/feart.2022.1001795

COPYRIGHT
© 2023 Kong, Wang, Yao, Lin, Xiao and
Yang. This is an open-access article
distributed under the terms of the
[Creative Commons Attribution License
\(CC BY\)](https://creativecommons.org/licenses/by/4.0/). The use, distribution or
reproduction in other forums is
permitted, provided the original
author(s) and the copyright owner(s) are
credited and that the original
publication in this journal is cited, in
accordance with accepted academic
practice. No use, distribution or
reproduction is permitted which does
not comply with these terms.

Petrology and geochemical characteristics of amphibolite facies rocks in Xunyangba area, South Qinling Orogen, Central China

Juanjuan Kong^{1,2}, Lei Wang^{3,4}, Yongxiang Yao⁵, Jinyan Lin^{3*},
Yuanyuan Xiao^{2,5,6*} and Yiting Yang¹

¹College of Ocean Science and Engineering, Shandong University of Science and Technology, Qingdao, China, ²Laboratory for Marine Geology, Qingdao National Laboratory for Marine Science and Technology, Qingdao, China, ³Department of Geology, Northwest University, Xi'an, China, ⁴Yanchang Oilfield Exploration and Development Technology Research Center, Yan'an, China, ⁵CAS Key Laboratory of Marine Geology and Environment, Institute of Oceanology, Chinese Academy of Sciences, Qingdao, China, ⁶Center for Ocean Mega-Science, Chinese Academy of Sciences, Qingdao, China

As a tectonic block of the Qinling Orogenic Belt, Central China, the South Qinling Orogen is generally believed to have had a tight affinity with the Yangtze Block during the Precambrian. Knowledge on the South Qinling Orogen is important to constrain the tectonic evolution of the northern margin of the Yangtze Block basement. Previous studies mainly focused on the east segment of the South Qinling Orogen. This paper presented petrological, geochronological, and geochemical studies on the amphibolite-facies rocks newly discovered in the middle section of the South Qinling Orogen. Geochemical studies indicate that the protolith of these amphibolites is calc-alkaline island arc basalt, which was formed during the reconstruction of the Paleo-Middle Archean crust on the northern margin of the Yangtze Block 2,362 ± 100 Ma ago (equivalent to metamorphic rocks of the Yudongzi group). Later, these arc basalts experienced amphibolite-facies metamorphism at 1,500–1,800 Ma, which is consistent with the metamorphism identified in the Yangtze Block, confirming the association of the South Qinling Orogen with the Yangtze Block basement. Subsequently, these amphibolite-facies rocks further experienced three stages of metamorphism at c. 800 Ma, 440 Ma, and 200 Ma in the context of the northward subduction of the Yangtze Block.

KEYWORDS

amphibolite, zircon U–Pb age, geochemical characteristics, Xunyangba area, Southern Qinling Orogen

1 Introduction

The Qinling Orogenic Belt (QOB) was formed by the collision between the North China Block (NCB) and the Yangtze Block (YZB) through a long and complex tectonic evolution history (Zhang et al., 2001, Figure 1). Among different sub-units, the basement of the South Qinling Belt (SQB) is similar to that of the YZB in many aspects, including similar geochronological and geological histories, and thus, the SQB is considered to have developed from the YZB (Zhang et al., 2001; Dong et al., 2011b; Wu and Zeng, 2012; Dong and Santosh, 2016). Therefore, knowledge on the SQB is important to better understand the tectonic evolution of the northern margin of the YZB.

The basement of the Yangtze Plate is composed of an ancient crystalline basement of amphibolite to granulite facies and a folded basement of greenschist facies. For the SQB, the Douling group (~2,000 Ma) and the Yaolinghe group (~800 Ma) represent the amphibolite-facies basement and the greenschist-facies basement, respectively. The Douling complex is the oldest crystalline basement of the SQB, which is mainly composed of biotite gneisses, amphibolites, schists, and marbles (Zhang et al., 1996; Shen et al., 1997; Zhang et al., 2004). Previous studies on the Douling complex mainly focused on the protolith age (Hao et al., 1996; Zhang et al., 2002; Hu et al., 2013; Wu et al., 2014; Nie et al., 2016), metamorphism age (Hu et al., 2013; Hu et al., 2019), tectonic attribution (Yang et al., 2011), and the Neoproterozoic magmatism (Bai et al., 2019; Nie et al., 2019). However, detailed petrology and geochemical studies on the Douling complex are limited (Zhang et al., 2001). Moreover, previous studies on the Douling complex mainly focused on the east segment of the SQO, and it lacks the constraints by those for the middle-west segment of the SQO (only by the Foping dome). In addition, the metamorphic basement rocks of the SQB are widely distributed as the Yudongzi group and Foping group in the Neoproterozoic (Ling et al., 2002; Ling et al., 2008; Ling et al., 2010; Shi et al., 2013). However, the genetic relationship between these two groups and their relationship with the Douling complex have not been thoroughly investigated. Thus, studies on amphibolite-facies basement rocks of the Douling group from the SQB are significant to better understand the tectonic evolution history of the SQB in the Neoproterozoic.

In this paper, the newly discovered amphibolite-facies rocks from the Xunyangba area in the middle section of the SQO are reported for the first time. Based on detailed geochronological and geochemical data, this study aims to provide more information on the tectonic evolution history of the SQO and its relationship with the YZB.

2 Geological background

The QOB is one of the largest orogenic belts in Asia (Zhang et al., 2001), linking the Kunlun and Qilian orogens

to the west and the Dabie–Sulu orogen to the east (Meng and Zhang, 2000; Ratschbacher et al., 2003). The Qinling Orogen is a multistage orogen with two sutures. The northern suture lies mainly along the Shangdan tectonic zone, whereas the southern suture is marked by the Mianlue ophiolite complex. It developed through a series of complex seafloor subduction and terrene collision events (Zhang et al., 2001; Ratschbacher et al., 2003; Wang et al., 2009; Wu and Zheng, 2012; Kang et al., 2022), ultimately completed as a result of the continental collision between the YZB and the North China Craton (NCC) along the Mianlue suture zone in the early Mesozoic (Dong et al., 2011a). The QOB is divided into the Southern Qinling Orogen (SQO) and the Northern Qinling Orogen (NQO) from south to north by the Mianlue and Shangdan sutures (Figure 1, Wu and Zeng, 2012). The study area is located in the SQO. The main lithostratigraphic units are the Bikou group, the Yaolinghe group, the Wudang group, and the Douling group. They mainly underwent metamorphic volcanic-sedimentary (Meso-Neoproterozoic), passive continental margin sedimentation (Sinian–Early Paleozoic), and epicontinental marine deposit (late Paleozoic–Middle Triassic). They generally underwent the metamorphism of greenschist- and amphibolite-facies metamorphism conditions (Zhang et al., 2001). It is to be noted that the rock complex we studied consists of amphibolite-facies gneisses, schists, amphibolites, and minor marbles. The P-T conditions of the Douling complex were estimated at 490–560°C and 6–7.5 kbar for the prograde metamorphic stage and 630–720°C and 8–11 kbar for the peak metamorphic stage (Hu et al., 2019). It is generally accepted that the SQO was formed by the complex and long evolution of the YZB in the late stage (Ling et al., 2008). Therefore, the study of the SQO is a key to understanding the tectonic evolution history of the northern margin of the YZB. The ancient crystalline basement in the SQO is the Douling group, which is located in the south of the Shangdan suture zone and mainly distributed in the Dadouling–Xixiatian area. Previous research studies on the Douling group mainly focused on this area, which is structurally located in the eastern section of the SQO. The Xunyangba area is located in the middle part of the SQO and close to the Shangdan suture, the boundary of the SQO. The discovery of metamorphic rocks in the Xunyangba area of the Douling group can provide more basement and tectonic evolution information for the SQO.

3 Samples and petrological characteristics

The studied area is located in Xunyangba Town, Ankang City, Shaanxi Province (Figure 1). It belongs to the

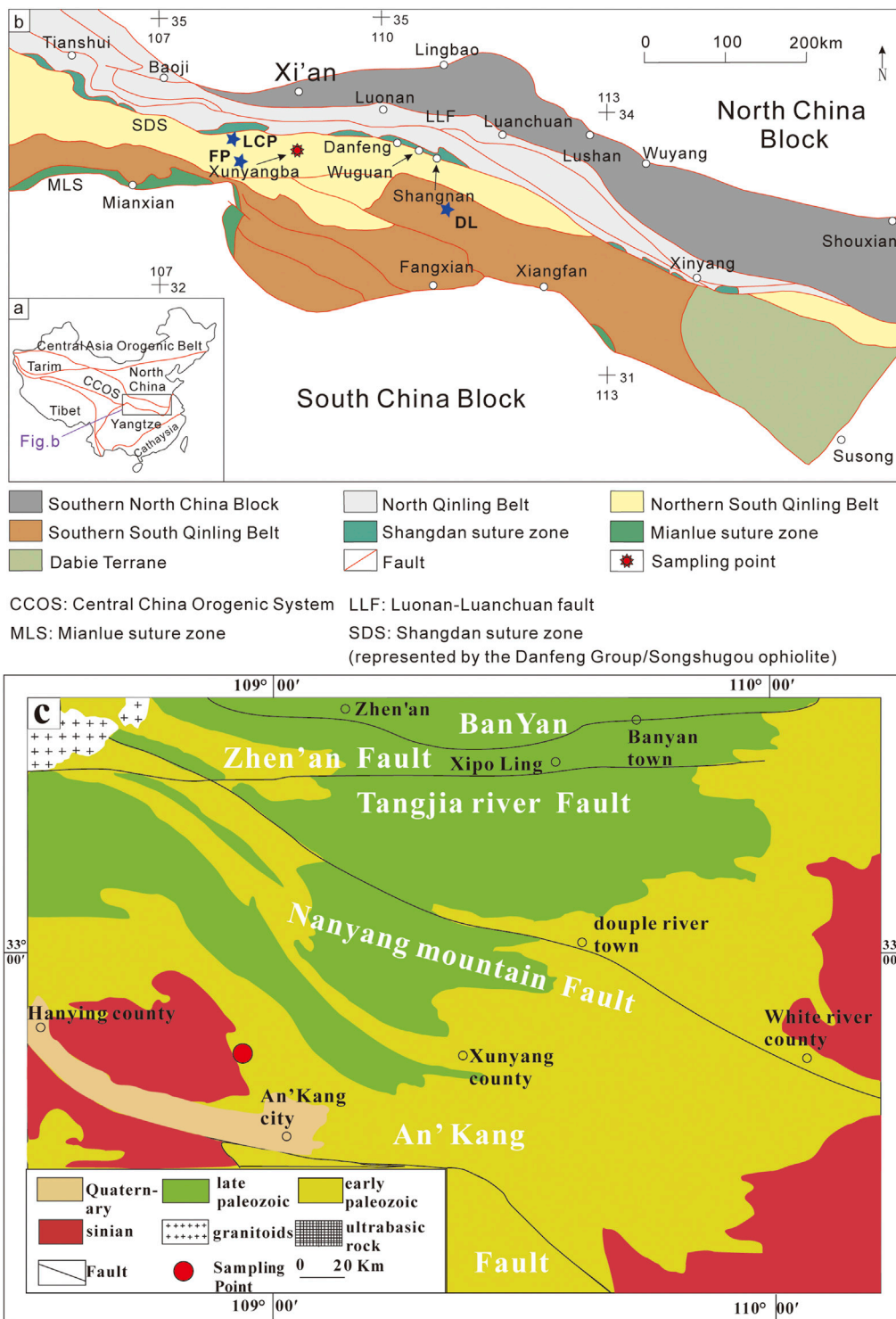


FIGURE 1 (A,B) Tectonic framework of Qinling Orogenic Belt (after Dong et al. (2011b) modified). LCP-Longcaoping group, FP-Foping group, DL-Douling group are from Zhang et al. (2001), (2021). (C) Tectonic framework of Xunyangba area (after Bai and Zhu (1984) modified).

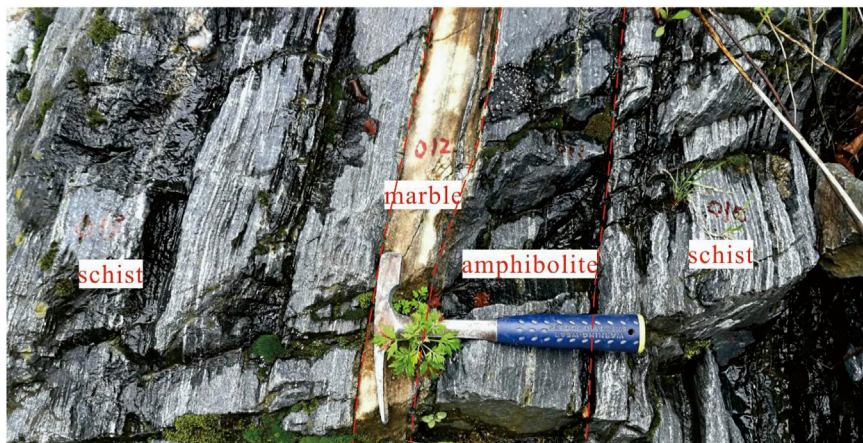


FIGURE 2
Lithological characteristics of the Xunyangba outcrop.

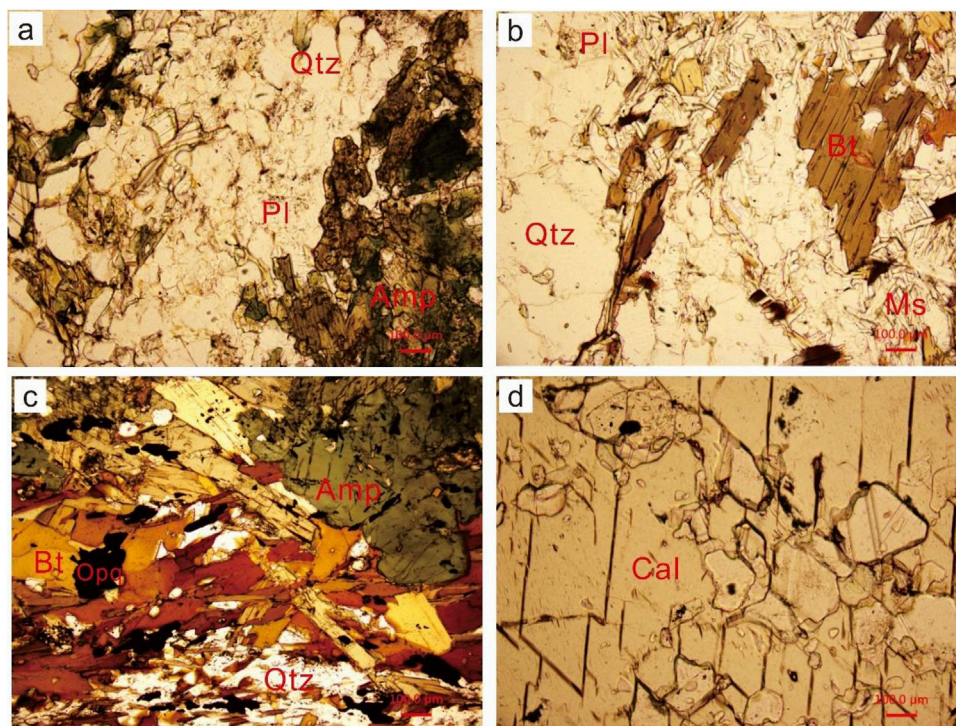


FIGURE 3
Microphotograph of metamorphic rocks in the Xunyangba area. (A) Amphibolite (plane-polarized light); (B) mica schist (plane-polarized light); (C) biotite schist (plane-polarized light); (D) marble (plane-polarized light). (Note: Mineral abbreviations that appear in this article are as follows: Amp = amphibolite, Bt = biotite, Cal = calcite, Chl = chlorite, Ep = epidote, Grt = garnet, Ms = muscovite, Pl = plagioclase, Qtz = quartz, and Opq = opaque mineral).

middle section of the SQO and lies between the Zhen'an-Banyan fault and the Shanyang-Fengzhen fault (Figure 1). The exposed metamorphic rocks mainly contain amphibolite,

schist, and marble (Figure 2). The amphibolite and schist are mainly banded, while the marble is banded or lenticular.

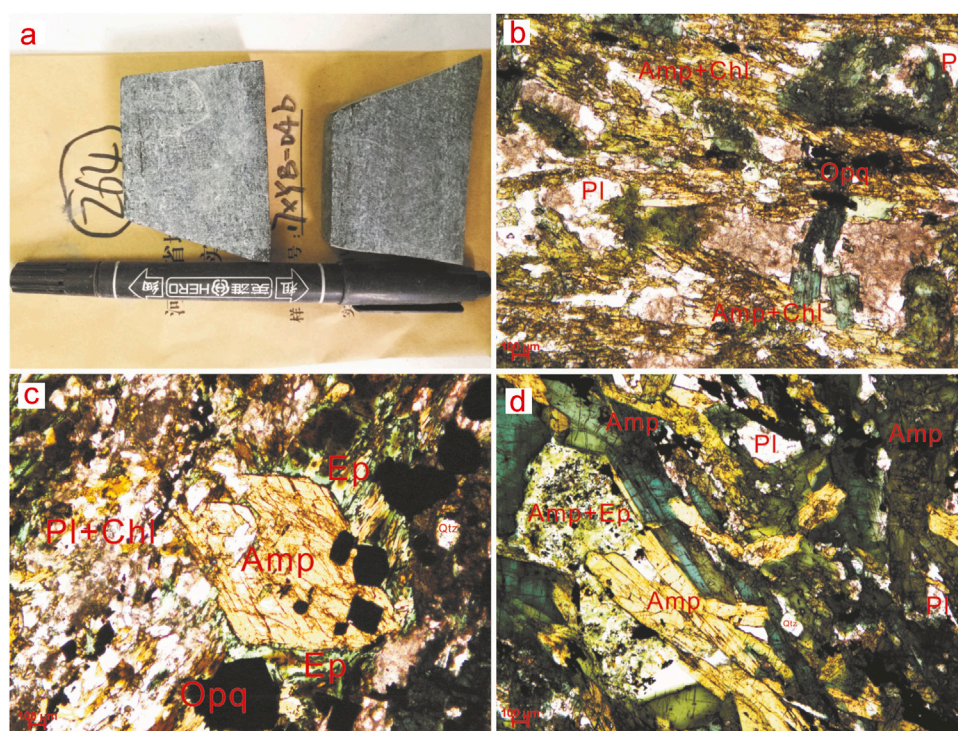


FIGURE 4

Photographs of typical amphibolite in the Xunyangba area (crossed-polarized light). (A) is the hand specimen of amphibolite. (B–D) are the microphotographs of the amphibolite (perpendicular-polarized light) (Note: Mineral abbreviations that appear in this article are as follows: Amp = amphibolite, Bt = biotite, Cal = calcite, Chl = chlorite, Ep = epidote, Grt = garnet, Ms = muscovite, Pl = plagioclase, Qz = quartz, and Opq = opaque mineral).

Amphibolite is mainly composed of amphibole and plagioclase with different modal amounts (Figure 3A; Figure 4). The schist is characterized by cleavage development and can be further divided into mica schist (Figure 3B), biotite schist (Figure 3C), hornblende biotite schist, biotite hornblende schist, and greenschist. Marble is medium and fine-grained with grayish white colors and a massive structure. The main composition of marble is carbonate minerals, which are euhedral granular with a particle size of 1–2 mm (Figure 3D). A small amount of biotite (10%) can also be seen in XYB-111. The lithology and mineral composition of the samples from the Xunyangba area are listed in Table 1.

4 Analytical methods

In this study, 21 representative samples from the Xunyangba area were analyzed for whole-rock major and trace element contents, eight of which were also analyzed for zircon U–Pb age dating and Hf isotope compositions. Weathered surfaces, pen, and saw marks were removed and thoroughly cleaned. Then, the rock chips were ultrasonically cleaned using the Milli-Q water and dried before powdering

into less than 200-mesh in a clean environment using an agate mill for analysis.

4.1 Zircon U–Pb

Zircon crystals were separated for U–Pb age dating using the heavy magnetic technique at the Laboratory of the Hebei Institute of Geological Surveying and Mapping. After plating carbon on zircon targets, cathodoluminescence (CL) scanning was completed by Chongqing Yujin Technology Co., Ltd. U–Pb dating was conducted using laser ablation inductively coupled plasma mass spectrometry (LA-ICP-MS) in the Laboratory of Ocean Lithosphere and Mantle Dynamics (LOLMD) at the Institute of Oceanology, Chinese Academy of Sciences (IOCAS), Qingdao. Zircons were ablated with an UP-193 Solid-State laser (193 nm, New Wave Research Inc.) (Xiao et al., 2020). Zircon 91500 was used as an external standard. The U–Th–Pb isotope ratio of zircon standard 91500 is recommended according to Wiedenbeck et al. (1995). The software of ICP-MS-Data-Cal was used for off-line data calibration for trace element analyses and U–Pb dating (Liu et al., 2010). Concordia diagrams and weighted mean age

TABLE 1 Mineral assemblages of studied metamorphic rocks from the Xunyangba area.

Sample	Lithology	Major mineral composition
XYB-01	Plagioclase amphibolite	Amp(65%)+Pl (20%)+Qz (10%)+Cal(<5%)
XYB-02	Plagioclase amphibolite	Amp(65%)+Pl (20%)+Qz (10%)+Bt+Cal(5%)
XYB-02b	Amphibolite	Amp(85%)+Pl (5%)+Qz (10%)+Bt (<5%)
XYB-03	Amphibolite	Amp(85%)+Pl (10%)+Qz (5%)+Bt (<5%)
XYB-04a	Mica schist	Qz (60%)+Bt (20%)+Ms (20%)
XYB-04b	Mica schist	Qz (60%)+Bt (20%)+Ms (20%)
XYB-05	Marble	Cal
XYB-06	Greenschist	Chl (70%)+Amp(30%)
XYB-07	Plagioclase amphibolite	Amp(65%)+Pl (20%)+Qz (10%)+Cal(<5%)
XYB-08	Biotite schist	Qz (55%)+Pl (15%)+Bt (25%)+Amp(<5%)
XYB-09	Hornblende biotite schist	Qz (55%)+Pl (5%)+Bt (30%)+Amp(10%)
XYB-10	Hornblende biotite schist	Qz (55%)+Pl (10%)+Bt (25%)+Amp(10%)
XYB-11	Amphibolite	Amp(80%)+Pl (5%)+Qz (10%)+Cal(<5%)
XYB-12	Marble	Cal
XYB-13	Hornblende biotite schist	Qz (50%)+Pl (10%)+Bt (30%)+Amp(10%)
XYB-13a	Biotite hornblende schist	Qz (50%)+Pl (10%)+Bt (10%)+Amp(30%)
XYB-14	Biotite schist	Qz (60%)+Pl (15%)+ Bt (5%)+Ms (15%)
XYB-15c	Biotite hornblende schist	Qz (50%)+Pl (10%)+Bt (10%)+Amp(30%)
XYB-15d	Biotite hornblende schist	Qz (50%)+Pl (10%)+Bt (10%)+Amp(30%)
XYB-16c	Biotite hornblende schist	Qz (50%)+Pl (10%)+Bt (10%)+Amp(30%)
XYB-16d	Biotite hornblende schist	Qz (55%)+Pl (5%)+Bt (10%)+Amp(30%)
XYB-17a	Biotite schist	Qz (60%)+Pl (10%)+Bt (25%)+Amp(<5%)
XYB-17b	Schist	Qz (75%)+Pl (10%)+Bt (5%)+Amp(5%)
XYB-18a	Biotite schist	Qz (60%)+Pl (15%)+Bt (20%)+Amp(<5%)
XYB-18c	Biotite schist	Qz (60%)+Pl (15%)+Bt (20%)+Amp(<5%)
XYB-19a	Schist	Qz (75%)+Pl (10%)+Bt (5%)+Amp(5%)
XYB-19b	Schist	Qz (80%)+Pl (5%)+Bt (10%)+Amp(5%)
XYB-20	Plagioclase amphibolite	Amp(60%)+Pl (20%)+Qz (10%)+Bt (5%)+Cal(5%)
XYB-111	Marble	Cal+Bt

Mineral abbreviations that appear in this article are as follows: Amp, amphibolite; Bt, biotite; Cal, calcite; Chl, chlorite; Ep, epidote; Grt, garnet; Ms, muscovite; Pl, plagioclase; Qz, quartz; Opaq, opaque mineral.

calculations were processed using Isoplot/Ex version 4.15 (Ludwig, 2012).

Sample preparation and analytical details are given in Chen et al. (2017).

4.2 Major and trace elements

Whole-rock major and trace element contents were analyzed using the Agilent 5100 inductively coupled plasma-optical emission spectrometer (ICP-OES) and the Agilent 7900 inductively coupled plasma mass spectrometer (ICP-MS), respectively, in LOLMD at IOCAS. The ICP-OES analytical precision is estimated to be better than 5%. Sample preparation and analytical details are given in Kong et al. (2019a). For trace element analysis, 50 mg of powder from each sample was dissolved with mixed HF and HNO₃ (1:1) in a high-pressure-jacketed Teflon beaker until complete digestion/dissolution. Analytical precision for most trace elements is better than 5%.

4.3 Hf isotope analysis of zircon

To ensure that the zircon U–Pb age corresponds to the result of Lu–Hf isotope analysis, the analyzed point for Hf isotope analysis was selected to be adjacent to the analyzed point for U–Pb age analysis. *In situ* Hf isotope analysis was carried out using a Geolas-193 laser-ablation system (Resolution M-50, ASI) attached to a Neptune MC-ICP-MS at the State Key Laboratory of Continental Dynamics, Northwest University. The beam size was set to be 43 μm with a 5 Hz repetition rate, and the laser energy density was 6 J/cm². Standard zircon 91500 and Mudtank were also measured during the sample analysis. The detailed analytical procedure and correction methods can be referred to in

TABLE 2 Major element contents (wt.%) and trace element contents (ppm) of metamorphic rocks from the Xunyangba area in this study.

Lithology	Amphibolite						Schist													Marble		
	Sample number	1	2	3	7	11	20	4	6	8	9	10	13	14	15	16	17	18	19	5	12	111
SiO ₂	48.43	44.70	45.85	44.47	49.16	46.26	72.79	35.74	49.18	42.70	49.43	49.86	76.24	47.52	89.85	63.39	80.27	82.19	5.69	19.99	31.14	
TiO ₂	3.40	2.30	1.94	2.77	1.68	2.88	0.60	1.10	1.94	1.91	3.32	2.65	0.36	1.37	0.28	1.32	0.41	0.35	0.06	0.26	0.33	
Al ₂ O ₃	13.81	16.55	16.16	13.71	13.61	16.73	12.13	11.10	15.41	13.60	15.53	16.27	13.59	16.10	2.92	14.07	8.38	6.84	0.37	1.76	5.53	
Fe ₂ O ₃	15.93	13.74	13.97	13.27	12.61	14.81	5.00	14.36	13.05	11.54	14.71	13.73	2.01	14.98	3.74	9.28	4.43	4.40	1.70	1.45	1.50	
MnO	0.19	0.21	0.19	0.20	0.26	0.21	0.05	0.09	0.28	0.18	0.21	0.21	0.04	0.24	0.28	0.33	0.31	0.32	0.15	0.13	0.03	
MgO	5.89	5.53	7.79	5.88	6.15	5.54	1.73	16.53	5.69	4.05	2.90	4.54	0.52	5.40	1.02	2.82	1.36	1.20	9.67	0.58	2.02	
CaO	7.62	10.22	8.42	12.01	12.35	8.43	0.69	9.95	6.91	12.71	7.87	6.87	0.66	8.77	1.36	1.80	1.14	2.52	39.78	42.95	32.46	
Na ₂ O	3.25	2.58	2.83	2.92	1.90	3.07	1.53	0.48	2.62	3.42	3.57	3.91	4.69	2.80	0.82	3.74	1.91	0.48	0.05	0.31	0.74	
K ₂ O	0.18	0.81	0.45	0.47	0.54	0.86	3.31	0.11	1.83	1.18	0.94	0.94	1.79	1.06	0.24	2.02	1.59	1.15	0.02	0.15	1.34	
P ₂ O ₅	0.23	0.33	0.21	0.29	0.18	0.35	0.15	0.11	0.30	0.42	0.76	0.42	0.10	0.22	0.17	0.12	0.11	0.10	0.12	0.11	0.12	
LOI	0.01	0.02	0.02	0.03	0.02	0.02	0.02	0.10	0.02	0.07	0.01	0.02	0.01	0.02	0.01	0.02	0.02	0.02	41.10	33.78	26.03	
Total	99.83	99.40	99.59	99.43	100.66	101.28	99.77	99.70	99.10	98.95	100.52	100.95	101.43	100.27	101.73	100.41	101.47	101.78	98.71	101.46	101.23	
Cs	0.96	5.52	14.59	1.33	1.22	2.62	3.14	2.42	9.48	2.49	2.86	2.75	0.82	1.72	1.10	5.30	2.28	3.38	0.09	0.10	2.90	
Rb	4.74	25.83	18.53	10.26	13.07	28.65	65.91	1.64	55.23	30.14	28.63	30.90	35.40	32.81	12.72	63.21	47.71	43.68	0.10	2.91	46.67	
Ba	31.60	304.40	47.11	334.36	97.68	101.87	728.37	7.57	672.44	197.32	246.13	177.45	995.58	248.39	367.04	1156.07	519.90	259.91	2.85	41.65	294.3	
Th	1.24	0.76	0.57	0.95	0.95	1.51	4.91	0.33	2.96	1.76	4.40	2.11	15.59	1.98	2.73	4.27	5.00	4.48	0.08	0.28	6.03	
U	0.39	0.21	0.16	0.58	0.31	0.45	1.25	0.15	0.66	0.57	0.92	0.45	3.34	0.34	0.24	0.63	0.75	0.89	0.06	0.30	1.63	
Nb	17.72	11.12	7.88	13.33	8.39	23.50	7.63	4.81	29.64	24.56	67.28	33.04	15.63	26.72	5.89	19.58	6.49	6.18	0.86	4.42	6.78	
Ta	1.23	0.76	0.52	0.89	0.55	1.47	0.57	0.34	1.79	1.49	3.97	2.01	1.19	1.53	0.36	1.23	0.47	0.43	0.06	0.26	0.51	
La	15.75	10.30	7.63	12.30	8.70	18.34	19.33	1.62	24.46	20.01	46.50	24.05	41.37	17.59	20.63	22.40	17.06	14.28	1.50	3.51	17.21	
Ce	39.58	26.01	19.94	31.19	21.67	42.41	39.96	5.01	52.16	46.15	102.52	53.29	81.33	36.76	39.90	56.25	41.99	36.81	3.12	6.87	29.30	
Pb	7.19	4.88	5.80	2.83	4.49	8.18	1.27	0.52	4.49	2.41	4.48	8.44	3.69	14.83	1.42	3.26	2.23	1.71	1.86	5.19	7.13	
Pr	5.57	3.71	2.95	4.52	2.99	5.60	4.59	0.87	6.32	6.06	12.86	6.53	8.58	4.10	6.05	6.19	4.22	3.66	0.52	1.00	3.69	
Mo	1.08	0.39	0.41	0.61	0.06	0.06	0.43	0.02	1.25	0.16	0.11	0.03	0.34	0.02	0.03	0.05	0.03	0.06	0.03	0.06	0.05	
Sr	324.65	296.20	189.06	225.37	464.78	436.26	45.42	29.86	274.40	313.69	335.10	492.78	61.02	653.90	60.15	124.75	65.69	76.72	424.69	270.57	3041.37	
Nd	26.17	17.79	14.56	22.08	14.12	25.48	17.73	4.28	26.34	26.71	54.69	27.81	30.74	16.49	26.69	25.52	17.10	14.61	2.52	4.49	14.14	
Sm	7.07	4.77	4.22	6.26	3.95	6.40	3.63	1.36	6.06	6.57	12.54	6.29	5.66	3.59	6.79	5.69	3.66	3.43	0.61	1.11	2.67	
Zr	154.85	88.69	84.50	126.25	64.06	114.98	133.28	37.59	153.86	173.92	325.42	190.98	219.84	56.72	53.09	194.46	95.96	86.11	6.62	41.33	102.75	
Hf	3.97	2.11	2.06	3.23	1.92	2.79	3.43	0.97	3.04	3.82	6.77	3.59	6.04	1.32	1.06	4.48	2.54	2.16	0.17	0.91	2.65	
Eu	2.30	1.79	1.55	2.07	1.36	2.16	0.87	0.58	2.16	2.10	3.82	2.23	0.91	1.26	1.62	1.56	0.88	0.79	0.21	0.34	0.56	
Ti	21424	14804	12455	17134	10592	17848	3755	4388	12058	11944	20704	16684	2290	8843	1774	8300	2555	2191	370	1405	2112	

(Continued on following page)

TABLE 2 (Continued) Major element contents (wt.%) and trace element contents (ppm) of metamorphic rocks from the Xunyangba area in this study.

Lithology	Amphibolite						Schist											Marble			
	Sample number	1	2	3	7	11	20	4	6	8	9	10	13	14	15	16	17	18	19	5	12
Gd	8.08	5.56	5.07	7.63	4.66	6.80	3.26	1.74	6.37	7.32	13.34	6.44	4.76	3.93	7.46	5.29	3.71	3.65	0.85	1.33	2.47
Tb	1.27	0.89	0.82	1.27	0.75	1.10	0.50	0.29	0.98	1.16	2.03	0.99	0.74	0.62	1.18	0.81	0.60	0.64	0.13	0.21	0.36
Dy	6.88	5.21	4.70	7.51	4.45	6.25	2.98	1.78	5.63	6.81	11.79	5.60	4.43	3.60	6.87	4.50	3.64	3.86	0.83	1.31	2.06
Li	12.21	21.26	27.26	23.31	7.52	26.89	41.42	27.44	42.09	23.48	13.13	24.12	15.79	20.89	6.55	34.35	22.22	14.65	2.40	1.47	28.98
Ho	1.38	1.11	1.01	1.63	0.94	1.34	0.63	0.38	1.20	1.45	2.49	1.18	0.96	0.77	1.47	0.90	0.81	0.86	0.22	0.30	0.44
Y	35.28	28.92	26.49	41.97	24.22	34.45	16.90	10.00	30.83	38.60	64.67	30.82	27.40	19.85	36.90	21.32	20.97	21.89	7.67	9.55	14.44
Er	3.59	3.09	2.85	4.67	2.65	3.71	1.89	1.06	3.38	4.15	7.05	3.30	2.96	2.17	4.17	2.45	2.42	2.52	0.74	0.91	1.27
Tm	0.47	0.43	0.39	0.63	0.36	0.50	0.28	0.15	0.45	0.56	0.97	0.43	0.43	0.29	0.60	0.32	0.33	0.35	0.11	0.13	0.18
Yb	2.80	2.67	2.48	3.95	2.17	3.06	1.74	0.98	2.79	3.51	6.04	2.65	3.01	1.85	4.08	2.08	2.29	2.39	0.70	0.79	1.13
Lu	0.38	0.37	0.36	0.58	0.31	0.44	0.28	0.15	0.41	0.52	0.89	0.38	0.47	0.25	0.66	0.32	0.36	0.37	0.12	0.13	0.17
∑REE	121.27	83.70	68.54	106.29	69.09	123.57	97.67	20.27	138.71	133.08	277.52	141.18	186.35	93.28	128.19	134.30	99.07	88.22	12.18	22.43	75.64
∑LREE	96.43	64.36	50.86	78.42	52.79	100.38	86.10	13.73	117.50	107.59	232.92	120.21	168.59	79.80	101.69	117.62	84.91	73.57	8.47	17.32	67.57
∑HREE	24.84	19.34	17.68	27.87	16.30	23.18	11.56	6.54	21.21	25.49	44.59	20.97	17.76	13.49	26.50	16.69	14.16	14.65	3.70	5.10	8.07
LREE/HREE	3.88	3.33	2.88	2.81	3.24	4.33	7.45	2.10	5.54	4.22	5.22	5.73	9.49	5.92	3.84	7.05	6.00	5.02	2.29	3.39	8.38
(La/Yb) _N	4.03	2.77	2.20	2.23	2.87	4.30	7.95	1.19	6.28	4.09	5.53	6.52	9.87	6.83	3.62	7.71	5.35	4.28	1.53	3.18	10.97
(La/Sm) _N	1.44	1.39	1.17	1.27	1.42	1.85	3.44	0.77	2.61	1.97	2.40	2.47	4.72	3.16	1.96	2.54	3.01	2.69	1.59	2.04	4.16
(Gd/Yb) _N	2.38	1.72	1.69	1.60	1.78	1.84	1.55	1.47	1.89	1.73	1.83	2.01	1.31	1.76	1.51	2.10	1.34	1.26	1.00	1.39	1.81
Eu/Eu*	0.93	1.06	1.02	0.92	0.97	1.00	0.77	1.15	1.06	0.93	0.90	1.07	0.54	1.03	0.70	0.87	0.73	0.68	0.89	0.86	0.67
Ce/Ce*	1.04	1.03	1.03	1.03	1.04	1.03	1.04	1.03	1.03	1.03	1.03	1.04	1.06	1.06	0.88	1.17	1.21	1.25	0.87	0.90	0.90
A	55.55	54.87	58.00	47.10	47.92	57.51	68.69	51.29	57.56	44.00	55.64	58.13	65.56	56.04	54.68	65.05	64.36	62.24	0.92	3.90	13.80
K	5.25	23.89	13.72	13.86	22.13	21.88	68.39	18.64	41.12	25.65	20.84	19.38	27.62	27.46	22.64	35.07	45.43	70.55	28.57	32.61	64.42
al	20.10	22.95	21.71	18.79	18.95	23.48	39.98	12.28	23.45	19.76	24.59	24.83	47.91	22.71	19.82	31.18	33.71	30.32	0.37	2.10	7.44
fm	51.67	44.16	50.82	44.00	44.61	46.62	35.75	66.70	47.86	36.66	41.83	44.73	13.84	46.72	52.50	43.12	38.41	40.36	26.94	4.16	9.52
c	20.16	25.78	20.56	29.93	31.27	21.51	4.16	20.02	19.12	33.57	22.67	19.08	4.23	22.47	16.76	7.24	8.31	20.29	72.57	92.95	79.46
alk	8.07	7.11	6.91	7.28	5.17	8.39	20.11	1.00	9.57	10.02	10.91	11.37	34.01	8.10	10.92	18.47	19.57	9.04	0.11	0.79	3.58
DF	-1.56	1.07	-2.29	2.22	-0.09	0.14	-3.74	-11.63	-1.02	6.43	2.56	1.12	1.46	-0.15	-8.55	-1.07	-4.90	-6.69			

a, fm, and calk are Nigil in value; DF, $10.44 - 0.21 \times \text{SiO}_2 - 0.32 \times \text{Fe}_2\text{O}_3 - 0.98 \times \text{MgO} + 0.55 \times \text{CaO} + 1.46 \times \text{Na}_2\text{O} + 0.54 \times \text{K}_2\text{O}$; Ce/Ce* = $\text{Ce}_N / (\text{La}_N \times \text{Pr}_N)^{1/2}$; Eu/Eu* = $\text{Eu}_N / (\text{Sm}_N \times \text{Gd}_N)^{1/2}$; the chondrite-normalized values are from Sun and Macdonough (1989).

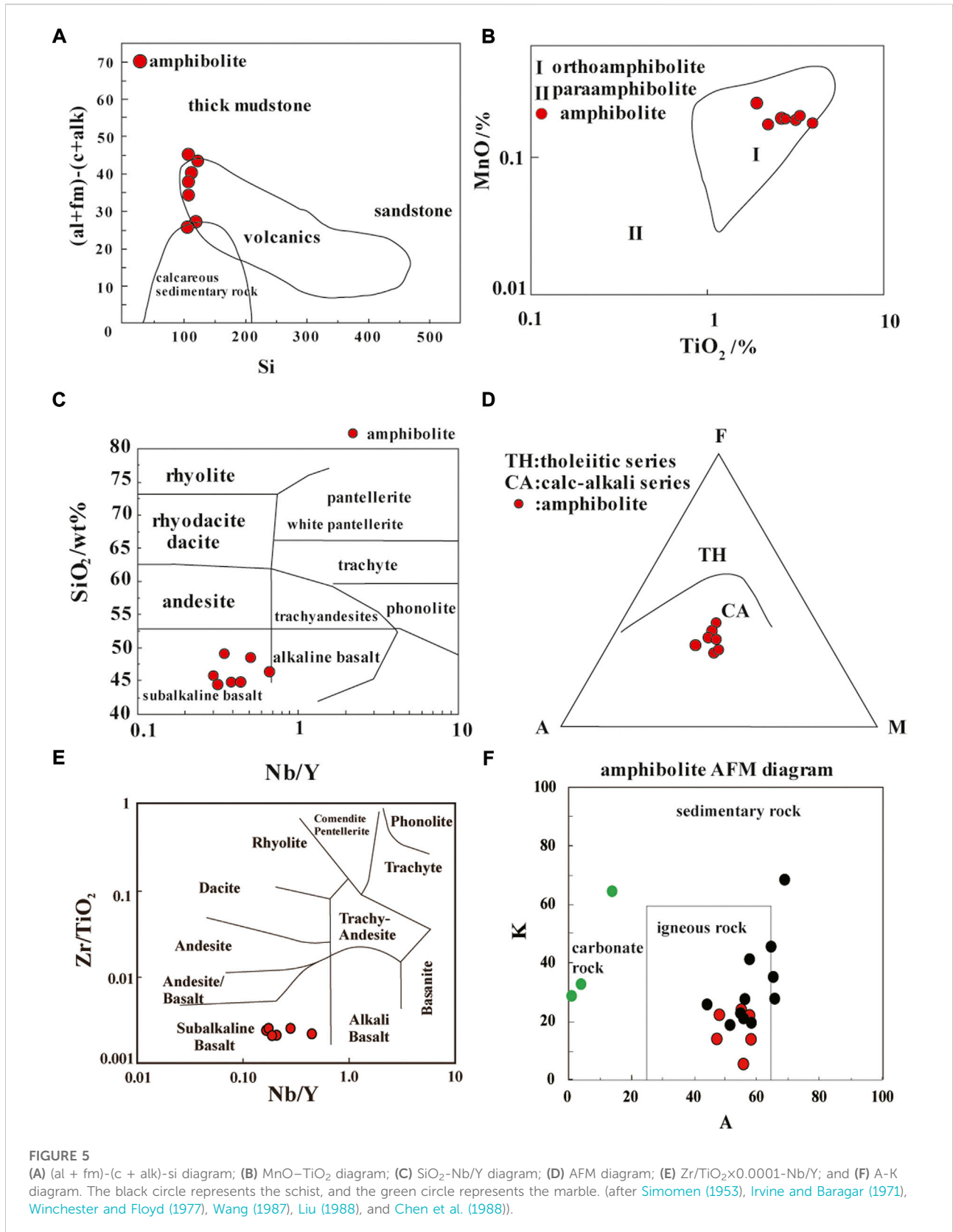
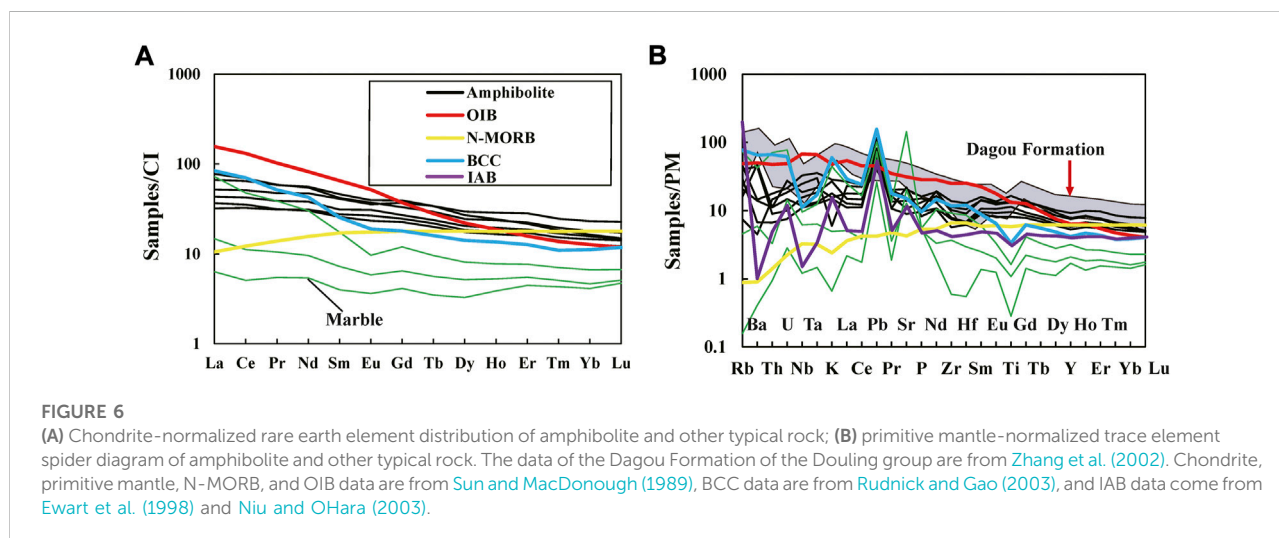


FIGURE 5
 (A) $(al + fm)-(c + alk)$ -si diagram; (B) MnO–TiO₂ diagram; (C) SiO₂–Nb/Y diagram; (D) AFM diagram; (E) Zr/TiO₂×0.0001–Nb/Y; and (F) A–K diagram. The black circle represents the schist, and the green circle represents the marble. (after Simomen (1953), Irvine and Baragar (1971), Winchester and Floyd (1977), Wang (1987), Liu (1988), and Chen et al. (1988)).

TABLE 3 Some element contents of metamorphic rocks from the Xunyangba area and other rocks in literature studies (the data are from Wang (1987); Liu (1988); and Li et al. (2006)).

Lithology	SiO ₂	TiO ₂	Al ₂ O ₃	Fe ₂ O ₃	MnO	MgO	CaO	Na ₂ O	K ₂ O	P ₂ O ₅
Oceanic island arc greywacke	58.53	1.06	17.11	7.27	0.15	3.65	5.83	4.10	1.60	0.26
Continental island arc greywacke	70.69	0.64	14.04	4.34	0.10	1.97	2.68	3.12	1.89	0.16
Active epicontinental greywacke	73.86	0.46	12.89	2.75	0.10	1.23	2.48	2.77	2.90	0.09
Stable terrigenous greywacke	81.95	0.49	8.41	2.95	0.05	1.39	1.89	1.07	1.71	0.12
Oceanic ridge tholeiite	49.80	1.50	16.00	9.30	7.50	11.20	2.80	0.14		
Island arc tholeiite	51.10	0.83	16.10	10.00	5.10	10.80	2.00	0.30		
Continental rift basalt	50.30	2.20	14.30	12.45	5.90	9.70	2.50	0.80		
Magmatic carbonate rock	7.60	0.21	1.15	0.65	0.50	1.85				
Sedimentary carbonate rock	13.4	0.12	1.88	0.19	0.47	0.19				
Quartz sandstone	96.90	0.06	1.71	0.44	0.75	0.39	0.40	0.47		
Amphibolite (average)	46.23	2.48	15.20	14.01	0.21	6.14	9.78	2.77	0.54	0.28
Marble (average)	18.94	0.22	2.55	1.55	0.10	4.09	38.40	0.37	0.50	0.11



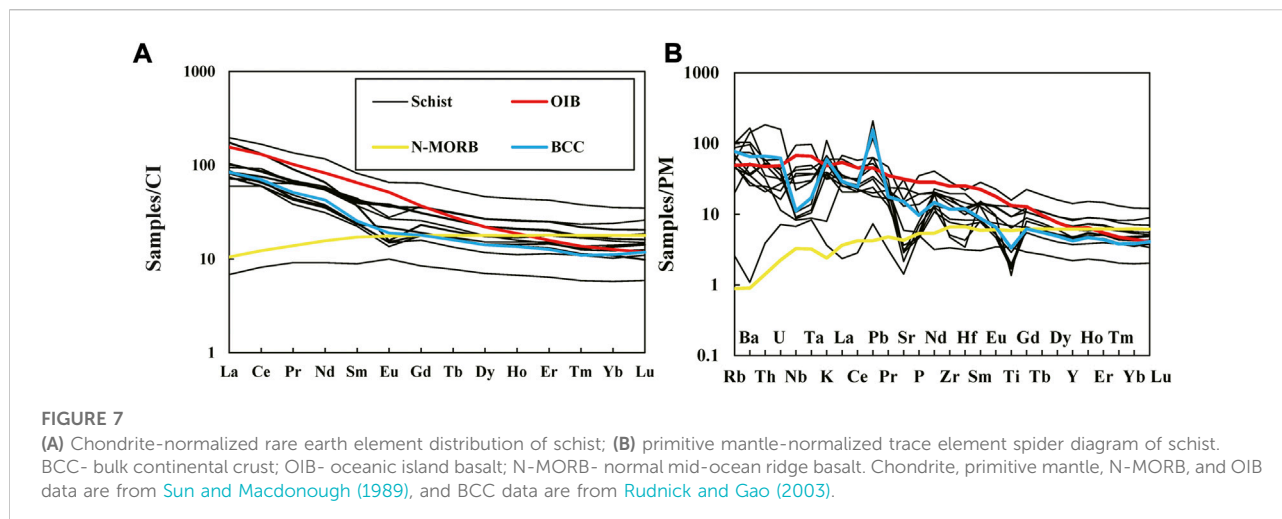
Yuan et al. (2008). The other reference parameters we used in this study are as follows: $(^{176}\text{Lu}/^{177}\text{Hf})_{\text{CHUR}} = 0.0332$, $(^{176}\text{Hf}/^{177}\text{Hf})_{\text{CHUR}} = 0.282772$, $(^{176}\text{Lu}/^{177}\text{Hf})_{\text{DM}} = 0.0384$, and $(^{176}\text{Hf}/^{177}\text{Hf})_{\text{DM}} = 0.28325$ (Blichert-Toft et al., 1997; Griffin et al., 2002). Herein, CHUR and DM represent the chondrite uniform mantle and depleted mantle, respectively.

5 Results

5.1 Major elements

The major element contents of metamorphic rocks from the Xunyangba area are shown in Table 2. Amphibolite is characterized by low alkali ($\text{K}_2\text{O} + \text{Na}_2\text{O}_{\text{average}} = 3.3 \text{ wt}\%$) and

high Fe (total Fe_2O_3 contents are 12.6–15.9 wt%) with $\text{Mg}^\#$ values of 26.99–35.80. Because most major elements (such as TiO_2 , MgO , P_2O_5 , and Al_2O_3) can be conserved during metamorphism, they can reflect the protolith composition (Bernard-Griffiths et al., 1985; Han, 2019). Thus, the high Fe and Mg of amphibolite are consistent with the characteristics of basalt, while the low K and Na can be affected by subsequent metamorphism. In the (al + fm) - (c + alk)-si diagram, the data are plotted in volcanic rock areas showing the characteristics of basic volcanic rocks (Figure 5A). In the $\text{MnO}-\text{TiO}_2$ diagram, they all fall in the ortho-amphibolite (Figure 5B). In the $\text{SiO}_2-\text{Nb}/\text{Y}$ diagram, they fall in the subalkaline basalt (Figure 5C). In the AFM diagram, they show the characteristics of the calc-alkaline series (Figure 5D).



For schist, SiO₂ contents are 35.7 wt%–89.9 wt%, Al₂O₃ is 2.9 wt%–16.3 wt%, MgO is 0.5 wt%–16.5 wt%, total Fe₂O₃ is 2.0 wt%–15.2 wt%, and K₂O + Na₂O is 0.6 wt%–6.5 wt%. The ratio of K₂O/ Na₂O varies from 0.15 to 2.39. That is, the schists are rich in Al and Fe, with a poor Mg that is basically with various SiO₂. A preliminary scan of the data allows us to divide the samples into three groups. These analyses show protoliths of the schists whose SiO₂ < 50 wt% are igneous rocks (Table 2 and Figure 5F). Also, most of the schists (50 < SiO₂ < 80 wt%) are very similar to the compositions of the continental island arc greywacke (Tables 2, 3, Supplementary Figure S2). The SiO₂ content in three samples XYB-16, 18, and 19 was > 80 wt%, containing quartz >75% with blastopsammitic texture, whose protolith should be stable terrigenous greywacke (Tables 2, 3, Supplementary Figure S2).

For marble, CaO is a major component (32.5 wt%–43.0 wt%). MgO contents vary greatly (0.6 wt%–9.7 wt%), which may reflect the varying contribution of the dolomite component. Total Fe₂O₃ is 1.45 wt%–1.70 wt%. SiO₂ is 5.7 wt%–31.1 wt%. According to its composition of major elements and the correlation of impurity composition, which indicate that the SiO₂ in the marble is not produced by the chemical deposit process. According to the content of P₂O₅ in carbonate rocks, magmatic carbonates and sedimentary carbonates can be distinguished. Because the P₂O₅ content of magmatic carbonates is in excess of 0.8 wt%, the P₂O₅ content of sedimentary carbonates is usually less than 0.8% (Liu, 1988). According to Table 3, P₂O₅ is 0.11 wt%, so we can judge that the protolith of marble in the Xunyangba area is sedimentary carbonates.

DF discriminant (Shaw, 1965; Shaw, 1972) is an effective method for distinguishing the protolith of metamorphic rocks. Together with the A-K diagram, the protoliths of metamorphic rocks from the Xunyangba area are further

confirmed, that is, carbonate rocks for marble, igneous rocks for amphibolite, and sedimentary rocks for some schist (Figure 5F).

5.2 Trace elements

The rare earth elements were conserved under the condition of ultrahigh pressure metamorphism, even if the amphibolite-facies metamorphism causes the change of large ion lithophilic elements (Green et al., 1969). Therefore, rare earth elements are often used as an important parameter to identify the protolith (Chen et al., 2014). It is generally believed that the metasedimentary rocks whose protolith are feldspathic rocks have higher LREE/HREE and an obvious negative Eu anomaly, while the metasedimentary rocks whose protolith are femic rocks have lower LREE/HREE and no negative Eu anomaly (Cullers and Podkovyrov, 2000).

High-field-strength elements (HFSEs) are relatively stable, insoluble in water, and not easily affected by metamorphism and late alteration; usually, they can be used to trace the provenance of metamorphic rocks (Feng and Kerrich, 1990; Qiu et al., 2013). HFSEs such as Nb and Ta of amphibolite in the profile are similar to E-MORB, and elements such as REE, U, and Zr are similar to IAB (Figure 6B). ΣREE of plagioclase amphibolite is 68.54 ppm–123.57 ppm. The distribution pattern of rare earth elements generally shows slight fractionation of light rare earth elements (La/Yb)_N = 2.20–4.30 and no Eu and Ce anomaly (Figure 6A) (δ_{Eu} is 0.92–1.06; δ_{Ce} is 1.03–1.04), which share similar characteristics with E-MORB. It is characterized by relative depletion of HFSE (Nb, Ta, and Th) and enrichment of LILE (Figure 6B), resembling those of basalt formed in an island-arc or back-arc setting. According to Winchester and Floyd (1977), immobile trace elements such as Ti, Zr, Nb, and Y indicate the

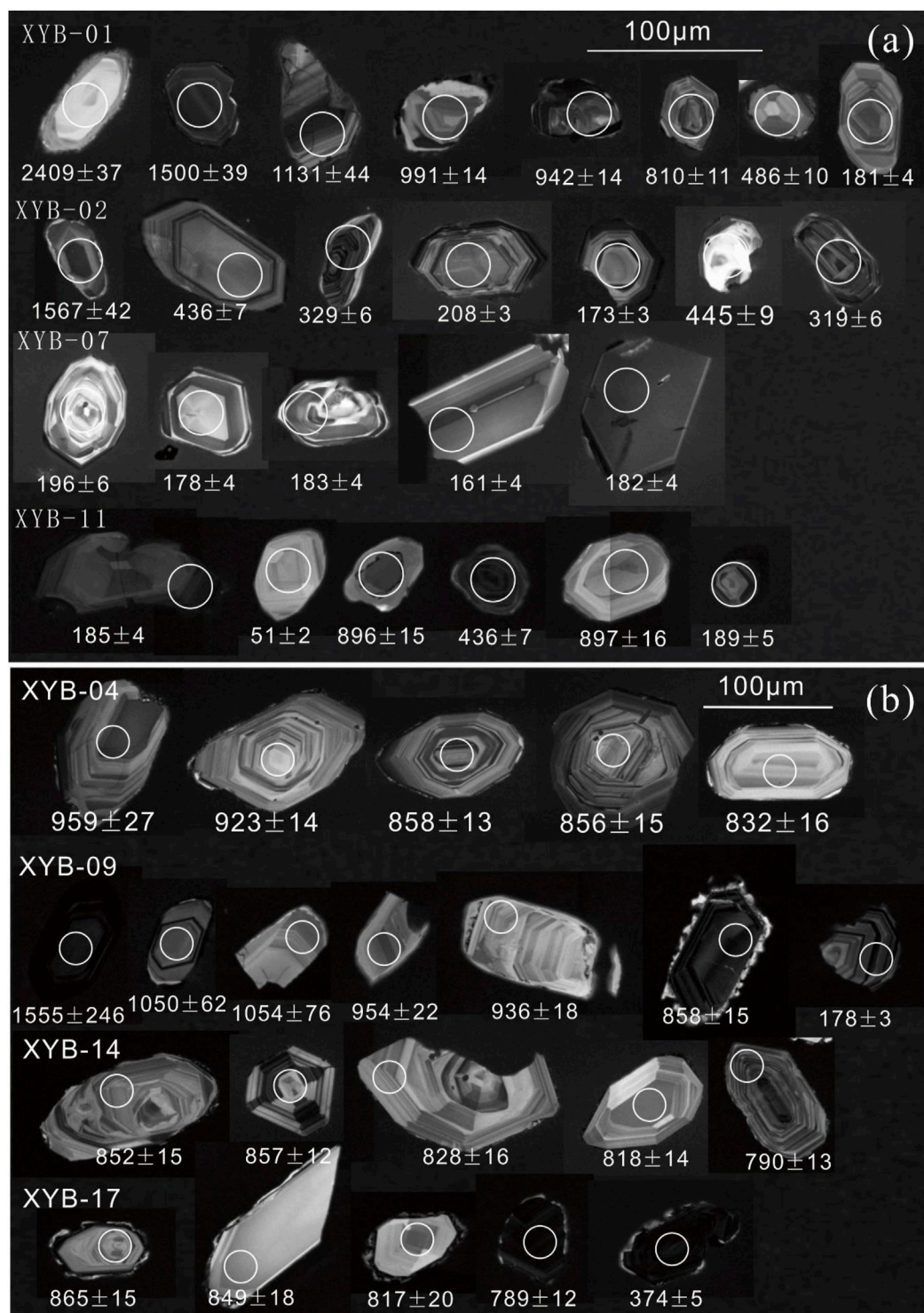


FIGURE 8
(A) Zircon cathodoluminescence image of amphibolite; **(B)** Zircon cathodoluminescence image of schist (age unit: Ma).

protolithic rocks, degree of differentiation, and possible tectonic settings. In the $Zr/TiO_2 \times 0.0001$ vs. Nb/Y (Figure 5E) diagrams, all amphibolite samples lie within the

subalkaline basalt field. Rb- and Ba-high anomalies indicate that the fluid involved in metasomatism during the generation of magma, which leads to the rocks becoming calc-alkaline.

TABLE 4 Isotope characteristics of metamorphic rocks from the SQO in literature studies.

Location	Sample	Chronological method	Age/Ma	References	
South of Xixia County	Gneiss	Sm-Nd model age	2,134	Shen et al. (1997)	
			2,118		
			2,096		
			2,122		
			2,144		
		Average	1,878 ± 256		
		Rb-Sr isochron age	422 ± 16		
		²⁰⁷ Pb/ ²⁰⁶ Pb	1,635 ± 22		
			1,672 ± 25		
		Average	1,657 ± 22		
		Plagioclase amphibolite	Sm-Nd model age		2,089
					2,097
					2,203
	2,188				
	2,250				
	Gneiss	Whole rock Sm-Nd isochron age Sm-Nd model age Average	1,878 ± 256	Zhang et al. (1996)	
			2,096–2144		
			2,123		
	Diopside granulite	Single-zircon evaporation dating method	2,519 ± 4		
			2,506 ± 3		
			2,457 ± 3		
2,020 ± 13					
1,840 ± 10					
Grey gneiss	Single-zircon evaporation dating method	1,918 ± 2			
		1,905 ± 5			
		787 ± 12			
Gangou quartz diorite	Sm-Nd model age Single-zircon evaporation dating method	2,014 ± 104			
		714 ± 9			
Diopside granulite	Sm-Nd model age Sm-Nd model age Average Zircon microprobe	725 ± 29	Zhang et al. (2004)		
		740 ± 6			
		1,842 ± 2			
		One 2,432 Others > 2.5Ga			
Xixia County, Xiaoyingou	Gneiss	Single-zircon evaporation dating method	1635 ± 22	Zhang et al. (2002)	
			1,672 ± 25		
			1,657 ± 22		
		Sm-Nd isochron age Sm-Nd model age	1,860 ± 350		
			2,096–2144		
Average 2123 ± 16	Plagioclase amphibolite	Rb-Sr isochron age Sm-Nd model age	463 ± 60		
			2,089–2,254		
Average 2197 ± 64		⁴⁰ Ar/ ³⁹ Ar	830 ± 30		

(Continued on following page)

TABLE 4 (Continued) Isotope characteristics of metamorphic rocks from the SQO in literature studies.

Location	Sample	Chronological method	Age/Ma	References
Xixia County, Wawuchang group	Diopside granulite	Rb–Sr isochron age	256	Zhang et al. (2002)
			235	
		Single-zircon evaporation dating method	1,840 ± 10	
			1,844 ± 45	
			1,842 ± 22	
			2,020 ± 13	
			2,457 ± 3	
			2,505 ± 5	
			2,507 ± 2	
			2,506 ± 3	
			2,519 ± 7	
			2,519 ± 5	
2,519 ± 4				
Xixia County, Dinghenan	Amphogneiss	Sm–Nd model age	1,890	Zhang et al. (2002)
			2,006	
			2,415	
		Average	2,014 ± 104	
		Single-zircon evaporation dating method	787 ± 12	
Xixia County, Daotiangou	Quartz diorite	Rb–Sr isochron age	862 ± 110	Zhang et al. (2002)
			Sm–Nd model age	
			1,840	
		Average	1,842 ± 2	
		Single-zircon evaporation dating method	714 ± 9	
			725 ± 29	
			740 ± 6	
			Average	

The total amount of rare earth elements in schist is relatively low ($\Sigma\text{REE} = 20.27\text{--}277.52$ ppm). The rare earth elements generally show a right-leaning descending type (Figure 7A; $(\text{La}/\text{Yb})_{\text{N}}$ is 1.19–9.87) and no Eu or little Eu anomaly (δ_{Eu} is 0.54–1.15) and no Ce or little Ce anomaly (δ_{Ce} is 0.88–1.21); some resemble those of BCC, and some are similar to N-MORB, which are consistent with major element characters. These schists are relatively rich in LILEs such as Rb, Ba, and K and have a relative depletion of HFSEs (Nb, Ta, and U), which are consistent with those of BCC (Figure 7B). Combined with the characteristics of petrology and major elements, it is inferred that the protolith of schist partially represents amphibolite, originating from the island arc and part greywacke, whose $\text{SiO}_2 > 70$ wt.% were derived from continental margins (Supplementary Figures S1, S2).

The marbles have relatively low levels of rare earth elements ($\Sigma\text{REE} = 12.18$ ppm–75.64 ppm; the average is 36.75 ppm, which is only 0.25% of the world's typical carbonate rocks) and show slight fractionation ($(\text{La}/\text{Yb})_{\text{N}} = 1.53\text{--}10.97$ and $(\text{Ga}/\text{Yb})_{\text{N}} = 1.00\text{--}1.81$, Figure 6A). It is obvious that there is a negative Eu anomaly ($\delta_{\text{Eu}} = \text{Eu}_{\text{N}}/(\text{Sm}_{\text{N}} \times \text{Gd}_{\text{N}})^{1/2} = 0.67\text{--}0.89$), relative enrichment of LILE (U and Ba), extreme depletion of Ti, and relative depletion of HFSE

(Nb, Ta, Zr, and Hf, Figure 6B). This is somewhat similar to commonly observed patterns for sedimentary carbonates (Boulvais et al., 2000). Also, the variable LILE abundances may be the result of metamorphic disturbance. Positive La, Gd, and Y anomalies and a negative Ce anomaly are completely similar to the characteristics of typically modern seawater (Horita et al., 1991). At the same time, it has obviously Th-poor and U-rich ($w(\text{U})/w(\text{Th}) < 1$) schists that are consistent with those of sedimentary carbonate. For marble whose protolith is sedimentary carbonates, the composition of paleoseawater determines the trace element characteristics of its protolith; second, the metamorphic diagenesis and the mixing of terrigenous clastic materials in the later period will influence the element content of marble (Zhen, 2014). It is believed that the total amount of REEs in sedimentary rocks increases with seawater depth, which can reflect the depth of seawater when the paleo-sediments form to some extent (Yang et al., 2008). The low total amount of rare earth elements (12.18–75.64 ppm) of the marble in the profile may indicate its formation in a shallow sea environment. Meanwhile, the contents of Th and Zr in carbonate rocks vary greatly with the mixing of terrigenous clastic materials (Taylor and McLennan, 1985). The Zr and Th elements of marble in the Xunyangba area vary greatly

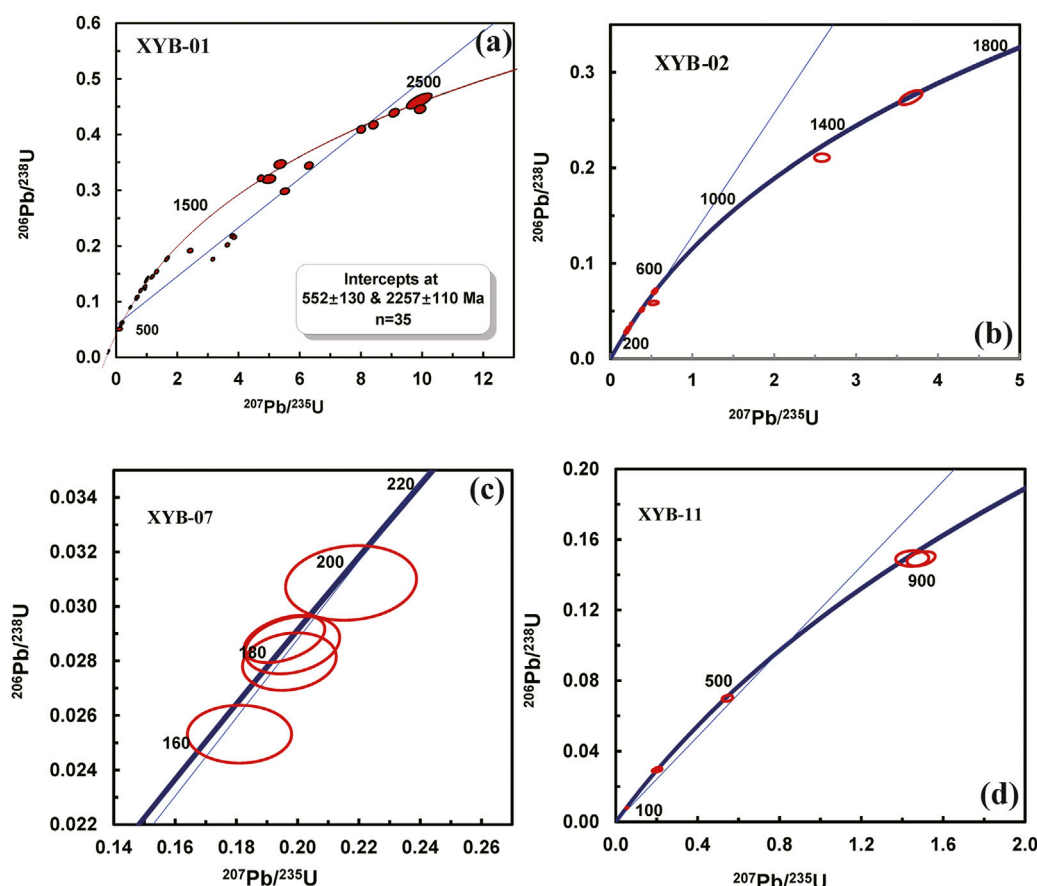


FIGURE 9

U-Pb age concordance of zircons of amphibolite for (A) XYB-01; (B) XYB-02; (C) XYB-07; (D) XYB-11.

(Table 2; Figure 6B). These results indicate that the protolith of the marble may be influenced by the terrigenous clastic materials, which are consistent with the observed petrological characteristics.

5.3 Zircon U–Pb chronology

LA-ICP-MS zircon U–Pb ages are given in [Supplementary Appendix SA](#) and shown on concordant plots in [Figures 8–10](#). The zircon age older than 1.0 Ga is denoted by $^{207}\text{Pb}/^{206}\text{Pb}$, and the zircon age younger than 1.0 Ga is denoted by $^{206}\text{Pb}/^{238}\text{U}$. The dating results of the metamorphic rocks of the Douling group are summarized in [Table 4](#).

5.3.1 Amphibolite

The CL images ([Figure 8A](#)) of zircons in amphibolites show that they are granular, rhombic, and long or short columnar, with a particle size of about 13–160 μm and a length–width ratio of about 3.5:1–1:1. Most zircons have a core and mantle structure, there are large zircon inheritance cores inside, and some zircons develop white metamorphic growth edges. Th content of the

zircon is 40.55 ppm–265.83 ppm, U content of the zircon is 96.86 ppm–209.44 ppm, and the Th/U ratio is 0.06–1.94.

A total of 35 zircons were selected from the sample XYB-01 for U–Pb dating. The ages of the upper and lower intersection points of the concordant curve are 2257 ± 110 and 552 ± 130 Ma ([Figure 9](#)). A total of 30 pieces of data represent five concentrated areas on the graph. For five data, all the measuring points are located in the core of zircon, and the $^{207}\text{Pb}/^{206}\text{Pb}$ age is 2264 ± 34 Ma– 2476 ± 34 Ma (weighted-average age: 2362 ± 100 Ma; MSWD = 5.9), which is interpreted as the time of intrusion of the protoliths of the amphibolite. In addition, the sample XYB-01 also contains a few zircons with the ages of $1,898 \pm 56$ Ma, $1,500 \pm 39$ Ma, 800–900 Ma, 440 Ma, and 200 Ma.

A total of 19 zircons were selected from the sample XYB-02 for U–Pb dating. One of the inherited zircons' $^{207}\text{Pb}/^{206}\text{Pb}$ ages is $1,567 \pm 42$ Ma. Two of the zircons yield $^{206}\text{Pb}/^{238}\text{U}$ ages of 436 ± 7 Ma and 445 ± 9 Ma ([Figure 9](#)). The remaining 16 zircons were late metamorphic or magmatic hydrothermal, whose $^{206}\text{Pb}/^{238}\text{U}$ ages concentrate on 173–329 Ma.

Five zircons were selected from the sample XYB-07 for U–Pb dating. $^{207}\text{Pb}/^{206}\text{Pb}$ weighted-average ages are 179 ± 14 Ma (N =

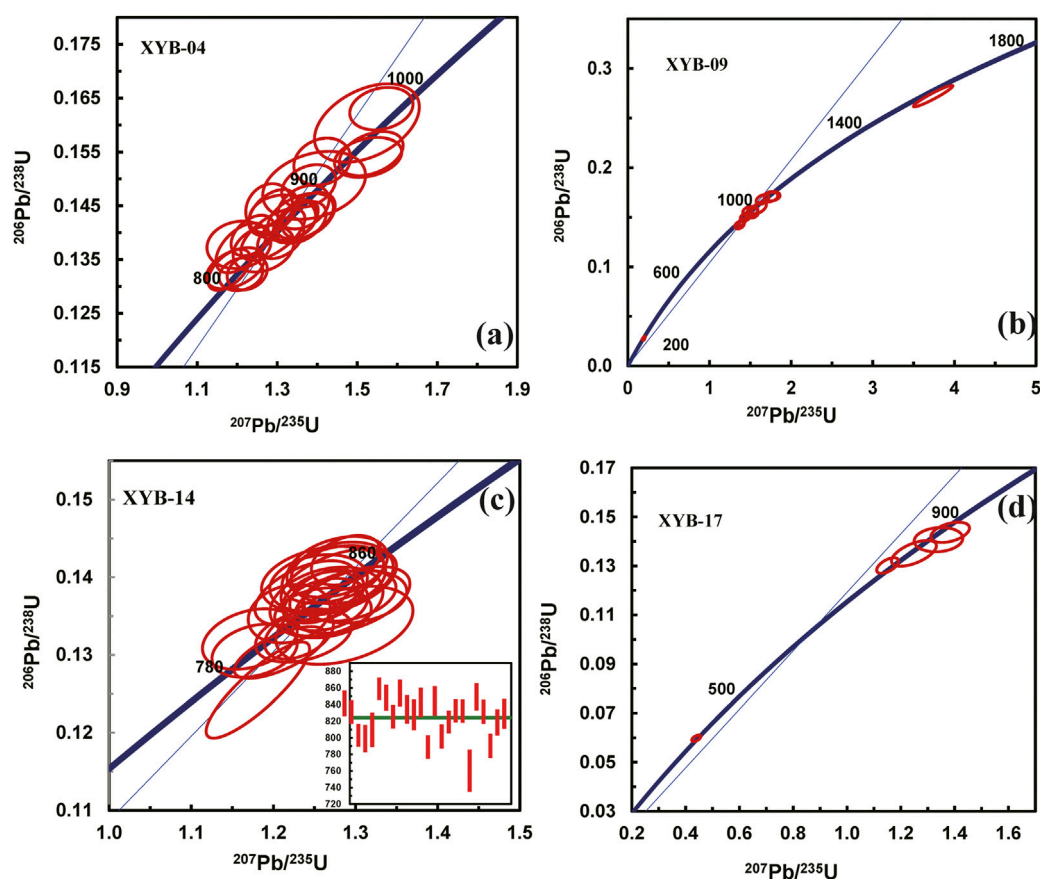


FIGURE 10 U-Pb age concordance of zircons of schist for (A) XYB-04; (B) XYB-09; (C) XYB-14; (D) XYB-17.

5, MSWD = 6.8) (Figure 9). These zircons are typical of magmatic rocks.

Six zircons were selected from the sample XYB-11 for U–Pb dating. It has two kinds of zircons: one is inherited, whose $^{206}\text{Pb}/^{238}\text{U}$ ages are 897 ± 16 Ma and 896 ± 15 Ma (Figure 9). The other magmatic zircon yields $^{206}\text{Pb}/^{238}\text{U}$ age of 436 ± 7 Ma. Three magmatic hydrothermal or metamorphic zircons yield $^{206}\text{Pb}/^{238}\text{U}$ ages of 185 ± 4 Ma, 189 ± 5 Ma, and 51 ± 2 Ma.

5.3.2 Schist

The CL images (Figure 8B) of zircons in schist show that they are rhombic and long or short columnar, with a particle size of about 65–150 μm and a length–width ratio of about 3:1–1:1. Most zircon-oscillating bands are clearly visible. The content of the zircon is 8.41 ppm–1,028 ppm, U content of the zircon is 13.04 ppm–361.6 ppm, and the Th/U ratio is 0.37–2.88.

A total of 26 zircons were selected from the sample XYB-04 for U–Pb dating. $^{206}\text{Pb}/^{238}\text{U}$ weighted-average ages are 859 ± 19 Ma ($N = 26$ and MSWD = 9.2) (Figure 10).

A total of 12 zircons were selected from the sample XYB-09 for U–Pb dating. One zircon is a magmatic zircon whose $^{207}\text{Pb}/$

^{206}Pb ages are $1,555 \pm 246$ Ma. Four magmatic zircons show $^{206}\text{Pb}/^{238}\text{U}$ weighted-average ages of 180 ± 9 Ma ($N = 2$ and MSWD = 2.2). Another nine zircons show $^{206}\text{Pb}/^{238}\text{U}$ weighted-average ages of 936 ± 11 Ma ($N = 9$ and MSWD = 14) (Figure 10).

A total of 24 zircons were selected from the sample XYB-14 for U–Pb dating. These zircons yield $^{206}\text{Pb}/^{238}\text{U}$ weighted-average ages of 824 ± 8.9 Ma ($N = 24$ and MSWD = 2.3) (Figure 10). They are made of magmatic zircon.

Five zircons were selected from the sample XYB-17 for U–Pb dating. One of these zircons is a metamorphic zircon. Another four magmatic zircons whose $^{206}\text{Pb}/^{238}\text{U}$ weighted mean ages are 823 ± 60 Ma ($N = 4$ and MSWD = 5.9) (Figure 10).

5.4 Zircon Hf isotope

Zircon Hf isotope analysis tested eight analysis points (see Supplementary Appendix SB). The initial value of $^{176}\text{Hf}/^{177}\text{Hf}$ is varied from 0.281116 to 0.282418 (the average value is 0.282029), $\epsilon_{\text{Hf}}(t)$ is -17.11 – -2.42 , $\epsilon_{\text{Hf}}(t)$ of analysis points is a negative value, and the T_{DM2} ages are 1,755–3,243 Ma. Two of the magmatic zircons

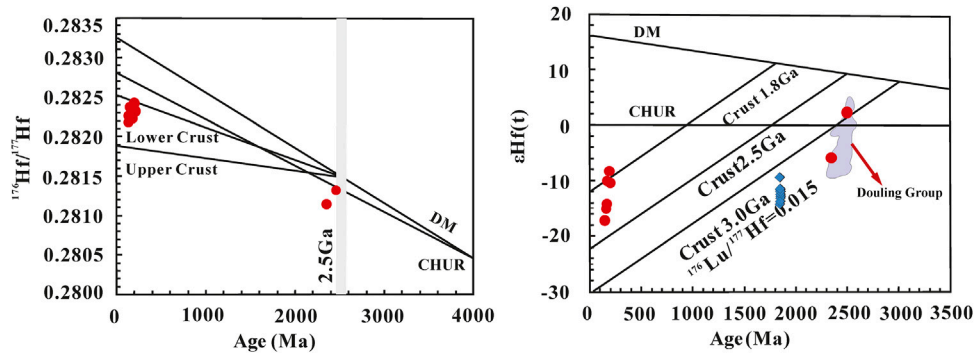


FIGURE 11

Zircon Hf isotope vs. age (Ma). CHUR-chondritic uniform reservoir; DM-depleted mantle. The blue rhombus squares represent the amphibolite of the Yudongzi group (Chen et al., 2019). The Douling group (Hu et al., 2013; Wu et al., 2014) in the previous study is used for comparison.

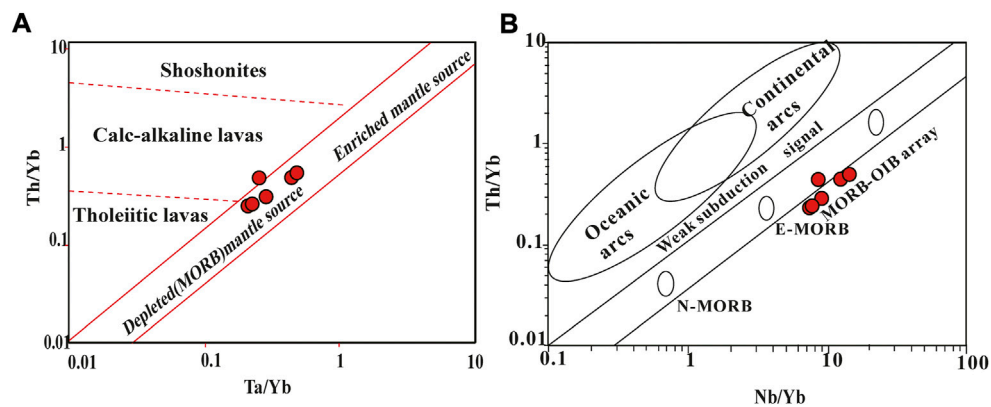


FIGURE 12

(A) Th/Yb-Ta/Yb (Alabaster et al., 1982) and (B) Th/Yb-Nb/Yb diagrams (Pearce, 2008). Red circle represents the amphibolite; E-MORB, enriched mid-ocean ridge basalt; MORB, mid-ocean ridge basalt; N-MORB, normal mid-ocean ridge basalt; OIB, ocean island basalt.

inherited from the protolith correspond to the T_{DM2} ages of 3,243 Ma and 2,847 Ma. It corresponds to two important continent growth periods (3.3–3.2 Ga and 2.95–2.90 Ga) in the YZB. According to the previous geochemical and petrological analyses, the protolith of amphibolite is a volcanic rock. Combining $\epsilon_{Hf}(t)$ is negative, which indicates that the amphibolite comes from the transformation and recycling of ancient crustal materials (Figure 11).

6 Discussion

6.1 Geochronology of the Douling group

The formation age of the metamorphic complex of the Douling group has been hotly debated. Shen et al. (1997) interpreted the U–Pb age of detrital zircons as 2.5 Ga by using single-grain zircon evaporation. The Sm–Nd isotope data constrained that the

metamorphic complex of the Douling group was formed in ~2,000 Ma (Yang et al., 2008). The study on gneiss of supracrustal origin found that the protolith formed in ~2,123 Ma, while sedimentation occurred very shortly followed by intense metamorphism at ~1,878 Ma (Zhang et al., 1996). Based on our study, the frequency distribution curve shows that amphibolite has several age peaks mainly at 2,476–2,311 Ma, 1,500–1,800 Ma, 800–900 Ma, ~440 Ma, and ~200 Ma. The protolith formation age of the plagioclase amphibolite is $2,362 \pm 100$ Ma. The ages of schist are mainly distributed in the Neoproterozoic (800–900 Ma), suggesting a strong metamorphic overprint, but no zircon greater than 1,600 Ma has been found in the schist. Because the schists share the same age spectrum peak with the amphibolite only after 1.0 Ga, it is speculated that they experienced the same metamorphism since 1.0 Ga.

Previous studies divided the Douling group into four groups based on the isotopic ages: (1) 2494 ± 27 Ma; (2) $1,657 \pm 22$ Ma– $1,931 \pm 89$ Ma; (3) ~850 Ma; and (4) 463 ± 60 Ma.

Additionally, the Rb–Sr age of the Dagou group was 325 Ma, and the Rb–Sr age of the Wawuchang formation was 256–235 Ma.

For the Douling group, Zhang et al. (2004) discovered that the ages of the single-grain zircon were 2.5 Ga in diopside granulites, which is interpreted as the residual age of rocks. In other areas, no age greater than 2.1 Ga has been found for protolith formation. Combined with the age data we obtained from amphibolite in the Xunyangba area, we find five zircons older than 2.1 Ga, yielding $^{207}\text{Pb}/^{206}\text{Pb}$ ages of $2,264 \pm 34$ Ma and $2,476 \pm 34$ Ma, with a weighted-average age of $2,362 \pm 100$ Ma ($n = 5$, MSWD = 5.9). The $\varepsilon_{\text{Hf}}(t)$ of these zircons is -17.11 – -2.42 , and the two-stage Hf model age is 1,755–3,243 Ma. Two magmatic zircons inherited from the protolith correspond to two-stage Hf model ages, that is, 2,847 Ma and 3,243 Ma. Coupled with the protolith of plagioclase amphibolite which is an arc basalt, the age $2,362 \pm 100$ Ma can be interpreted as the emplacement age of magma. The protolith was formed at $2,362 \pm 100$ Ma, which is different from the formation age (2.0 Ga) of the protolith obtained by Zhang et al. (2002). The age of the second group in the Xunyangba area was 1,500–1,800 Ma, which is consistent with the Sm–Nd isochron age of $1,860 \pm 350$ Ma and the zircon dating of $1,657 \pm 22$ Ma obtained from gneisses in Xixia County by Zhang et al. (2002). It represents metamorphism at the first stage. The third group is 800–900 Ma, which is similar to the $^{40}\text{Ar}/^{39}\text{Ar}$ age of plagioclase amphibolite in the Xiaoyingou of Xixia County and the single-grain zircon evaporation age of amphibogneiss in the Dinghenan of the Douling group. This represents a primary metamorphism occurring in the Douling group around 800 Ma. The fourth group is ~ 440 Ma, which is proven by the Rb–Sr age of gneiss in the south of Xixia County and Xiaoyingou. The fifth episode of arc-continent collision is caused by the northward subduction of the Paleo-Tethyan oceanic crust, resulting in low-P metamorphism in the Qinling Orogen at ca. 320–310 Ma and crustal accretion to the NCB (Wu and Zheng, 2012), which can be used to explain the Rb–Sr age ~ 325 Ma of the Dagou group. In the Xunyangba area, the peak age of the sixth phase is ~ 200 Ma, which is similar to the Rb–Sr age of diopside granulite of the Wawuchang formation in Xixia County. At this stage, the NCC collided with the Qinling Orogenic Belt, and abundant granitoids were produced in the SQO, which is also consistent with the U–Pb age of some zircons of Xunyangba metamorphic rocks.

6.2 Tectonic affinity of Xunyangba metamorphic rocks

The protolith of amphibolite-facies rocks in the Xunyangba area is a set of greywacke, carbonate rocks, and basic rocks. The protolith of amphibolite was formed at $2,362 \pm 100$ Ma. The greywacke and carbonate are deposited later than 1,800 Ma and earlier than 800 Ma. Some scholars argue that the YZB in the early Proterozoic

was in an environment of the island arc (Lu, 1986). The amphibolite may have formed in the island arc environment of the YZB during this period, which is consistent with the fact that the SQO has the same mantle evolution and Pb isotopic composition as the YZB. Zhang et al. (2002) believed that the Qinling Orogen experienced large-scale closure in 1,000–800 Ma and the SQO was subducted into the YZB. The deposition and metamorphism of island arc greywackes and carbonate rocks may have occurred at this time. Subsequently, the Douling group participated in the integration of small blocks in the Qinling Orogen (Zhang et al., 1996), became the basement of the Qinling microplate, and participated in the later tectonic evolution.

The Douling and Foping constitute the nucleus of the YZB, recording a common ~ 2.0 Ga orogenic event that integrated the YZB into the supercontinent Columbia (Bader et al., 2013). Moreover, Liu et al. (2018) found that the zircon records of 2,700–2,500 Ma were common in rocks of the Douling complex, and the material source of the Foping group aged at $\sim 2,467$ Ma may be closely related to the Douling group. Thus, it is necessary to compare the Xunyangba metamorphic rocks of the Douling group with the Foping group. First, the Xunyangba area is close to the Foping group (Figure 1), and both of them belong to the mid-northwest margin of the SQO. The formation age of the Foping group has not been determined, but it is certain that the formation of the Foping group is earlier than the intrusion of the Longcaoping group (Figure 1, in Foping County near the Foping group, 2,506 Ma), which is earlier than the formation of Xunyangba amphibolite. In terms of geochemistry, the Eu of the Foping group shows no obvious negative anomaly, which is consistent with the amphibolite of Xunyangba. In addition, the $(\text{La}/\text{Yb})_{\text{N}}$ of the Foping group is 19.55, the $(\text{La}/\text{Yb})_{\text{N}}$ of the Longcaoping group is 33.77 (Chang et al., 1998), and the $(\text{La}/\text{Yb})_{\text{N}}$ of Xunyangba amphibolite is 3.06. In terms of the major and trace elements, such as TiO_2 , MgO, Ta, and Hf in the Foping group, they greatly differ from those in Xunyangba metamorphic rock (Supplementary Figure S3). According to the high Nb of Longcaoping gneiss, whose protoliths are considered basic, this is consistent with Xunyangba amphibolite. Chronologically, the Foping group was formed in the late Archean (Li et al., 2000) that is slightly earlier than Xunyangba amphibolite, while the intrusion time of the Longcaoping group is equivalent to the formation age of amphibolite in the Xunyangba area. Additionally, the metamorphic rock series of Xunyangba underwent the tectonic thermal events in the later period: 1,500–1,800 Ma, 800–900 Ma, ~ 440 Ma, and ~ 200 Ma are closed to Longcaoping gneiss (1,200 Ma, 800 Ma, 400 Ma, and 200 Ma, Zhang et al., 2004). The main components of the Foping metamorphic crystalline rock series may be the metamorphic products of volcanic rocks formed from

mantle magma similar to MORB in the early Proterozoic (Zhang et al., 2004). In the Ta/Yb-Th/Yb diagram (Figure 12A), amphibolites may have come from the enriched mantle source. In the Nb/Yb-Th/Yb diagram (Figure 12B), amphibolites plot near MORB-OIB and the continental arc array, indicating that the protoliths of both groups are generally enriched calc-alkaline basalts, likely arc basalts, without ruling out the possibility of an OIB protolith. Although they share the similarity of the formation ages and tectonic thermal events in the later period, they show different geochemical characteristics (Supplementary Figure S3). It is difficult to infer a more detailed connection between Foping and Xunyangba metamorphic rocks.

The newly discovered metamorphic rocks in the Xunyangba of the Douling group are located in the middle part of the SQO and can be compared with other metamorphic rocks of the Douling group in the eastern part of the SQO. (1) The protolith age of Xunyangba amphibolite was 2362 ± 100 Ma, which is equivalent to the Paleoproterozoic (~ 2.5 Ga) obtained in amphibolite of the Douling group (Nie et al., 2016) and the emplacement age (2.47–2.51 Ga) obtained in granitic gneiss (Zhu et al., 2011); the metamorphic age of late tectonic transformation of Xunyangba metamorphic rock appeared in 1,500–1800 Ma, 800–900 Ma, 440 Ma, and 200 Ma, which was also found in the Douling group (Zhu et al., 2011; Nie et al., 2016). (2) The lithologic compositions are similar; all of them have plagioclase amphibolite and marble, and the protoliths of the metamorphic volcanic rocks in the Douling group and the amphibolite rocks in Xunyangba are all basic. Hao et al. (1996) believed that the Douling complex was an island arc basement in the late Proterozoic to the middle Sinian. The Sm–Nd isochronal age of 979 Ma was measured in the Gangou quartz diorite (Zhang et al., 2002), which can represent the intrusion age of intermediate acid intrusive rocks in the Douling group, which may have supplied the heat to the metamorphism of Xunyangba metamorphic rock in the 800–900 Ma. (3) The trace element diagram for Xunyangba amphibolite is similar to the Dagou formation of the Douling group (Figure 6B). (4) They share the same Hf isotopic composition (Figure 11B), that is, the zircon U–Pb ages of amphibolite-facies metamorphic rocks in the Xunyangba area are similar to those of other metamorphic rocks in the Douling group in the eastern part of the SQO, and the geochemical characteristics are also comparable.

It is generally considered that the SQB was a part of the YZB of South China during Precambrian times (Ling et al., 2008; Ling et al., 2010; Wang et al., 2013). This limited old basement, known as the Yudongzi group, Kongling complex, provides valuable information about the Archean tectono-magmatic evolution of the YZB and is useful for a better comparison between the SQO and the YZB. Compared with metamorphic rocks of the Yudongzi group as the basement of the YZB, we find that the major element content of MgO and Al₂O₃ and the HFSE content

such as Ta, Zr, and Hf of the metamorphic rocks of Xunyangba are similar to those of the Yudongzi group (Supplementary Figure S3). For the Nd model age of 3017 ± 69 Ma measured in gneiss of the Yudongzi group, a similar age has also been found in Xunyangba amphibolite (the T_{DM2} ages of the zircons in Xunyangba amphibolite were 2,847 Ma and 3,243 Ma). Furthermore, the metamorphic rocks of the Yudongzi group were formed at 2657 ± 100 Ma (Zhang et al., 2001), and the age of 2.5 Ga was constrained by the orthogneiss of the Douling group (Shi et al., 2013). The $\epsilon_{Hf}(t)$ of Xunyangba amphibolite is -17.11 – -2.42 . The amphibolites, overprinted by metamorphism at ~ 1.85 Ga in the Yudongzi terrane, are also similar to those of the Xunyangba amphibolites (Figure 11B). In combination with the above, it is reasonable to infer that the Xunyangba metamorphic rocks are equivalent to the composition of the Yudongzi group. This is different from the Kongling complex in the northern margin of the YZB, which records magmatic activities at ~ 3.2 – 3.3 Ga, ~ 2.9 Ga, and ~ 2.6 – 2.7 Ga (Chen et al., 2013; Guo et al., 2014; Nie et al., 2016).

6.3 The tectonic relationship of the South Qinling Orogen with the Yangtze Plate

It has been documented that the SQO shared a similar geological history with the YZB during the Precambrian (Ling et al., 2002; Ling et al., 2008; Ling et al., 2010). Major evidence comes from the similarity in Neoproterozoic magmatism (Dong et al., 2011b; Hu et al., 2019) and the age patterns of detrital zircons from Neoproterozoic sedimentary rocks (Ling et al., 2010). Our new data provide insights into the evolution of the SQO. Its relationship with the YZB is also evaluated. The formation of Xunyangba amphibolite may be related to the intense geological event of $\sim 2,500$ Ma in the SQO. Considering the SQO subducted into the YZB in $\sim 2,500$ Ma (Zhang et al., 2002), amphibolite may have been formed in an island arc environment, which was formed by the basement reconstruction (similar to the composition of the Yudongzi group) in the northern margin of the YZB. Subsequently, it participated in the tectonic evolution as the part of the northern margin of the YZB. In the middle Proterozoic, there was a strong expansion of volcanic activity in the YZB, which is confirmed by the zircon U–Pb age of 1,800–1,500 Ma in Xunyangba amphibolite. In the 1,000–800 Ma, the crystallization massif uniting occurred in Bashan of the southern YZB, and the uniting of small blocks occurred in the Qinling Orogen (Zhang et al., 2001). The Xunyangba metamorphic rock series probably formed the Qinling microplate basement by joining these small blocks and experienced metamorphism in 800–840 Ma as evidenced by the zircon U–Pb ages of amphibolite and schist (Figure 8). In the Neoproterozoic (~ 800 Ma), the SQO had subducted into the YZB (Zhang et al., 2002). During this period, the protolith

of sedimentary rocks also formed by deposition and became symbiotic with the basic rocks. The P-T metamorphic conditions of the Douling complex were estimated to be 490–560°C and 6–7.5 kbar for prograde metamorphism and 630–720°C and 8–11 kbar for the peak metamorphic condition (Hu et al., 2019), corresponding to a geothermal gradient of c. 20°C/km. The P-T conditions are similar to the Barrovian-type metamorphic belts that were formed by crustal thickening in a collisional environment. In the ~440 Ma (Dong et al., 2011b), the Xunyangba metamorphic rocks on the northern margin of the YZB underwent another phase of metamorphism. After ~440 Ma, the YZB subducted toward the NCB and the SQO as a passive continental margin, which accepted the deposition of the early Devonian marine sediments. Afterward, the Mianlue Basin was closed in the Qinling Orogen in the late Triassic (~220–200 Ma) (Kong et al., 2017; Kong et al., 2019b), and the orogenic belt was uplifted to become mountains by comprehensive collision, and metamorphism occurred as the fourth stage. Finally, in the Meso-Cenozoic, with the effects of tectonic extrusion and strike-slip of the SQO, the basement rocks at the depths in the Xunyangba area were exposed to the surface.

7 Conclusion

Based on new petrologic, geochemical, geochronological, and Hf isotopic data on the rocks from the Xunyangba area of the SQO in this study, together with literature data, we arrived at the following conclusions:

- (1) The protolith of amphibolites from the Xunyangba area is island arc calc-alkaline basalts, and the magma has been strongly contaminated by the crust during the uprising.
- (2) Zircon dating results indicate that the protolith of amphibolite from the Xunyangba area was formed in $2,362 \pm 100$ Ma through island arc magmatism and was the reconstructed product of the Paleo-Mesozoic crustal rocks (equivalent to the metamorphic rocks of the Yudongzi group). Then, metamorphism occurred at 1,500–1,800 Ma during the subduction of the SQO into the YZB.
- (3) For schist and marble of the Xunyangba metamorphic series, the depositional processes may have occurred during the subduction of the SQO into the YZB before 859 ± 19 Ma.
- (4) After the deposition, both basalts and sedimentary rocks of the Xunyangba metamorphic series have undergone three stages of metamorphism at 800–900 Ma, 440 Ma, and 200–220 Ma. The $\epsilon_{\text{Hf}}(t)$ of zircon is -17.11–-2.42, of which the magmatic zircons inherited from the protolith correspond to the T_{DM2} ages of 3,243 Ma and 2,847 Ma. These ages are in response to two important growth periods of the Yangtze continental crust (3.3–3.2 Ga and 2.95–2.90 Ga) and indicate that the SQO and YZB might have experienced the same crustal history.

Data availability statement

The datasets presented in this study can be found in online repositories. The names of the repository/repositories and accession number(s) can be found in the article/Supplementary Material.

Author contributions

The authors confirm that the manuscript has been read and approved by all named authors and that there are no other persons who satisfied the criteria for authorship but are not listed. They further confirm that the order of authors listed in the manuscript has been approved by all of us. They understand that the corresponding author is the sole contact for the editorial process. He/she is responsible for communicating with the other authors about progress, submissions of revisions, and final approval of proofs signed by all authors as follows: JK, LW, YoY, JL, YX and YiY.

Funding

This work was supported by the Special funds of Shandong Province to the Qingdao National Laboratory for Marine Science and Technology (2022QNLM050201), National Natural Science Foundation of China (Grant number 41776069 to YX), special project of strategic leading science and technology of the Chinese Academy of Sciences (Grant number: XDB42020302), and Natural Science Foundation of Shandong Province (NSFSP, grant number ZR2020QD044 to JK).

Acknowledgments

The authors particularly thank Fengtao Fang, Nan Han, and Peishan Sui for assistance with sample preparation and analysis.

Conflict of interest

The authors declare that the research was conducted in the absence of any commercial or financial relationships that could be construed as a potential conflict of interest.

Publisher's note

All claims expressed in this article are solely those of the authors and do not necessarily represent those of their affiliated organizations, or those of the publisher, the

editors, and the reviewers. Any product that may be evaluated in this article, or claim that may be made by its manufacturer, is not guaranteed or endorsed by the publisher.

Supplementary material

The Supplementary Material for this article can be found online at: <https://www.frontiersin.org/articles/10.3389/feart.2022.1001795/full#supplementary-material>

SUPPLEMENTARY FIGURE S1

REE-La/Yb (modified from Allègre et al. (1978)), black circle represents the schist in Xunyangba area.

References

- Alabaster, T., Pearce, J. A., and Malpas, J. G. (1982). The volcanic stratigraphy and petrogenesis of the Oman ophiolite complex. *Contr. Mineral. Pet.* 81 (3), 168–183. doi:10.1007/BF00371294
- Allègre, C. J., and Minster, J. F. (1978). Quantitative models of trace element behavior in magmatic processes. *Earth Planet. Sci. Lett.* 5, 1–25. doi:10.1016/0012-821X(78)90123-1
- Bader, T., Ratschbacher, L., Franz, L., Yang, Z., Hofmann, M., Linnemann, U., et al. (2013). The heart of China revisited, I. Proterozoic tectonics of the Qin mountains in the core of supercontinent Rodinia. *Tectonics* 32 (3), 661–687. doi:10.1002/tect.20024
- Bai, H. S., and Zhu, J. X. (1984). *Geological study of Hg-Sb deposit of gongguan in xunyang county, Shaanxi Province*. China: Library of China University of Geosciences, 1–66.
- Bai, Z. A., Shi, Y., Liu, X. J., Huang, Q. W., and Qin, K. L. (2019). Geochronology, geochemistry and Hf isotopes of Fengzishan pluton in South Qinling and its geological significance. *Earth Sci.* 44 (4), 1187–1201. doi:10.3799/dqkx.2018.586
- Bernard-Griffiths, J., Peucat, J. J., Cornichet, J., Leon, M. I. P. d., and Ibaguchi, J. G. (1985). U-Pb, Nd isotope and REE geochemistry in eclogites from the Cabo Ortegal complex, Galicia, Spain: an example of REE immobility conserving MORB-like patterns during high-grade metamorphism. *Chem. Geol. Isot. Geosci. Sect.* 52 (2), 217–225. doi:10.1016/0168-9622(85)90019-3
- Blichert-Toft, J., Chauvel, C., and Albarède, F. (1997). Separation of Hf and Lu for high-precision isotope analysis of rock samples by magnetic sector-multiple collector ICP-MS. *Contributions Mineralogy Petrology* 127 (3), 248–260. doi:10.1007/s004100050278
- Boulvais, P., Fourcade, S., Moine, B., Gruau, G., and Cuney, M. (2000). Rare-Earth elements distribution in granulite-facies marbles: a witness of fluid-rock interaction. *Lithos* 53, 117–126. doi:10.1016/S0024-4937(00)00013-X
- Chang, H., Wang, X. L., and Neng, W. (1998). Composition of basement of foping dome in South Qinling. *Northwest Geol.* 19 (3), 6–11.
- Chen, G. Y., Sun, D. S., and Yin, H. A. (1988). *Genetic mineralogy and prospecting mineralogy*. China: Chongqing Publishing House.
- Chen, K., Gao, S., Wu, Y. B., Guo, J. L., Hu, Z. C., Liu, Y. S., et al. (2013). 2.6–2.7 Ga crustal growth in Yangtze craton, south China. *Precambrian Res.* 224, 472–490. doi:10.1016/j.precamres.2012.10.017
- Chen, Q. A., Sun, M., Zhao, G. C., Zhu, W. L., Long, X. P., Wang, J., et al. (2019). Episodic crustal growth and reworking of the Yudongzi terrane, South China: Constraints from the Archean TTGs and potassic granites and Paleoproterozoic amphibolites. *Lithos* 326–327, 1–18. doi:10.1016/j.lithos.2018.12.005
- Chen, S., Wang, X., Niu, Y., Sun, P., Duan, M., Xiao, Y., et al. (2017). Simple and cost-effective methods for precise analysis of trace element abundances in geological materials with ICP-MS. *Sci. Bull. (Beijing)*. 62, 277–289. doi:10.1016/j.scib.2017.01.004
- Chen, Y. X., Pei, X. Z., Li, R. B., Li, Z. C., Pei, L., Liu, C. J., et al. (2014). Geochemical characteristics and tectonic significance of meta-sedimentary rocks from Naiji Tal group, eastern section of East Kunlun. *Geoscience* 28 (3). doi:10.3969/j.issn.1000-8527.2014.03.005
- Cullers, R. L., and Podkovyrov, V. N. (2000). Geochemistry of the mesoproterozoic lakhanda shales in southeastern yakutia, Russia: Implications for mineralogical and provenance control, and recycling. *Precambrian Res.* 104 (1), 77–93. doi:10.1016/S0301-9268(00)00090-5
- Dong, Y. P., Zhang, G. W., Neubauer, F., Liu, X. M., Genser, J., and Hauzenberger, C. (2011a). Tectonic evolution of the Qinling orogen, China: review and synthesis. *J. Asian Earth Sci.* 41, 213–237. doi:10.1016/j.jseaes.2011.03.002
- Dong, Y. P., Liu, X. M., Santosh, M., Zhang, X., Chen, Q., Yang, C., et al. (2011b). Neoproterozoic subduction tectonics of the northwestern Yangtze Block in South China: Constrains from zircon U-Pb geochronology and geochemistry of mafic intrusions in the Hannan Massif. *Precambrian Res.* 189, 66–90. doi:10.1016/j.precamres.2011.05.002
- Dong, Y. P., and Santosh, M. (2016). Tectonic architecture and multiple orogeny of the Qinling orogenic belt, central China. *Gondwana Res.* 29, 1–40. doi:10.1016/j.gr.2015.06.009
- Ewart, A., Collerson, K. D., Regelous, M., Wendt, J. I., and Niu, Y. (1998). Geochemical evolution within the Tonga-Kermadec-Lau arc-back-arc systems: the role of varying mantle wedge composition in space and time. *J. Petrology* 39 (3), 331–368. doi:10.1093/ptro/39.3.331
- Feng, R., and Kerrich, R. (1990). Geochemistry of fine-grained clastic sediments in the archaic abitibi greenstone belt, Canada: Implications for provenance and tectonic setting. *Geochim. Cosmochim. Acta* 54, 1061–1081. doi:10.1016/0016-7037(90)90439-R
- Green, T. H., Brunfelt, A. O., and Heier, K. S. (1969). Rare Earth element distribution in anorthosites and associated high grade metamorphic rocks, Lofoten-Vesterdaalen, Norway. *Earth Planet. Sci. Lett.* 7 (2), 93–98. doi:10.1016/0012-821X(69)90020-X
- Griffin, W. L., Wang, X., Jackson, S. E., Pearson, N., O'Reilly, S. Y., Xu, X., et al. (2002). Zircon chemistry and magma mixing, SE China: *In-situ* analysis of Hf isotopes, tonglu and pingtan igneous complexes. *Lithos* 61, 237–269. doi:10.1016/S0024-4937(02)00082-8
- Guo, J. L., Gao, S., Wu, Y. B., Li, M., Chen, K., Hu, Z. C., et al. (2014). 3.45 Ga granitic gneisses from the Yangtze craton, south China: Implications for early archaic crustal growth. *Precambrian Res.* 242, 82–95. doi:10.1016/j.precamres.2013.12.018
- Han, N. (2019). Proto-rock restoration and basin-mountain coupling analysis of metamorphic rocks in Tianshan mountains. Doctoral dissertation. Southwest Xinjiang (China): Northwestern University.
- Hao, J., Li, Y. J., Liu, X. H., and Zhu, X. R. (1996). The Douling paleo-island arc and wudang paleo-back arc basin in east Qinling and their geological significance. *Regional geology of China* 1, 43–50.
- Horita, J., Friedman, T. J., Lazar, B., and Holland, H. D. (1991). The composition of Permian seawater. *Geochim. Cosmochim. Acta* 55 (2), 417–432. doi:10.1016/0016-7037(91)90001-1
- Hu, J., Liu, X. C., Chen, L. Y., We, Q., Li, H. K., and Geng, J. Z. (2013). A 2.5 Ga magmatic event at the northern margin of the Yangtze craton: Evidence from U-Pb dating and Hf isotope analysis of zircons from the Douling Complex in the South Qinling orogen. *Chin. Sci. Bull.* 58 (28/29), 3564–3579. doi:10.1007/s11434-013-5904-1
- Hu, J., Liu, X. C., Qu, W., and Chen, L. Y. (2019). Mid-Neoproterozoic Amphibolite facies metamorphism at the northern margin of the

- Yangtze Craton. *Precambrian Res.* 326, 333–343. doi:10.1016/j.precamres.2017.10.010
- Irvine, T., and Baragar, W. (1971). A guide to the chemical classification of the common volcanic rocks. *Can. J. Earth Sci.* 8 (5), 523–548. doi:10.1139/e71-055
- Kang, W. B., Li, W., Dong, Y. P., Zhang, L., Zhao, J. X., and Sheir, F. (2022). Multi-stage metamorphism and deformation of the north qinling orogenic belt: Constraints from petrology, geochronology, and structural analysis of the qinling complex. *Gondwana Res.* 105, 201–216. doi:10.1016/j.gr.2021.09.007
- Kong, J., Niu, Y., Duan, M., Xiao, Y., Zhang, Y., Guo, P., et al. (2019b). The syn-collisional granitoid magmatism and crust growth during the West Qinling Orogeny, China: Insights from the Jiaochangba pluton. *Geol. J.* 54, 4014–4033. doi:10.1002/gj.3368
- Kong, J., Niu, Y., Duan, M., Zhang, Y., Hu, Y., Li, J., et al. (2017). Petrogenesis of luchaba and wuchaba granitoids in Western qinling: geochronological and geochemical evidence. *Mineral. Pet.* 111, 887–908. doi:10.1007/s00710-017-0501-7
- Kong, J., Niu, Y. L., Sun, P., Xiao, Y. Y., Guo, P. Y., Hong, D., et al. (2019a). The origin and geodynamic significance of the Mesozoic dykes in eastern continental China. *Lithos* 332/333, 328–339. doi:10.1016/j.lithos.2019.02.024
- Lai, S. C., and Zhang, G. W. (1996). Geochemical features of ophiolites in mianxian-lueyang suture zone, qinling orogenic belt. *J. China Univ. Geosciences* 7, 165–172.
- Li, B. T., Zhang, X. W., and Wang, C. (2006). Reconstruction of protoliths of metamorphic rocks and tectonic setting of the Haiyuan group in the Haiyuan in the eastern segment of the North Qilian mountains, China. *Geol. Bull. China* 25 (1), 194–203. doi:10.3969/j.issn.1671-2552.2006.01.031
- Li, S. G., Jagoutz, E., Chen, Y., and Li, Q. L. (2000). Sm-Nd and Rb-Sr isotopic chronology and cooling history of ultrahigh pressure metamorphic rocks and their country rocks at Shuanghe in the Dabie Mountains, Central China. *Geochim. Cosmochim. Acta* 64, 1077–1093. doi:10.1016/S0016-7037(99)00319-1
- Ling, W. L., Duan, R. C., Liu, X. M., Chen, J. P., Mao, X. W., Peng, L. H., et al. (2010). U-Pb dating of detrital zircons from the Wudangshan group in the North Qinling and its geological significance. *Chin. Sci. Bull.* 55 (22), 2440–2448. doi:10.1007/s11434-010-3095-6
- Ling, W. L., Gao, S., Ouyang, J. P., Zhang, B. R., and Li, H. M. (2002). Time and tectonic setting of the Xixiang group: Constraints from zircon U-Pb geochronology and geochemistry. *Sci. China Ser. D-Earth. Sci.* 45 (9), 818–831. doi:10.1007/BF02879516
- Ling, W. L., Ren, B. F., Duan, R. C., Liu, X. M., Mao, X. W., Peng, L. H., et al. (2008). Timing of the wudangshan, Yaolinghe volcanic sequences and mafic sills in South qinling: U-Pb zircon geochronology and tectonic implication. *Sci. Bull.* 53 (14), 2192–2199. doi:10.1007/s11434-008-0269-6
- Liu, T. (1988). Criterion distinguishing magmatic carbonatite and sedimentary carbonate rocks by rock-forming elements. *Mineral Rocks* (2), 53–63. doi:10.19719/j.cnki.1001-6872.1988.02.006
- Liu, Y., Gao, S., Hu, Z., Gao, C., Zong, K., and Wang, D. (2010). Continental and oceanic crust recycling-induced melt-peridotite interactions in the trans-north China orogen: U-Pb dating, Hf isotopes and trace elements in zircons from mantle xenoliths. *J. Petrology* 51, 537–571. doi:10.1093/petrology/egp082
- Liu, Z. H., Luo, M., Chen, L. Y., Qu, W., and Liu, X. C. (2018). Stratigraphic framework and provenance analysis in the foping area, the south qinling tectonic belt: constraints from LA-ICP-MS U-Pb dating of detrital zircons from the metasedimentary rocks. *Acta Pet.* 34 (5), 1484–1502.
- Lu, L. Z. (1986). The Metamorphic rock series of China and its relation to crustal evolution. *J. Jilin Univ. (Earth Sci. Ed.)* (2), 1–14.
- Ludwig, K. (2012). *User's manual for Isoplot version 3.75-4.15: a geochronological toolkit for microsoft*. USA: Excel Berkeley Geochronological Center Special Publication.
- Meng, Q. R., and Zhang, G. W. (2000). Geologic framework and tectonic evolution of the Qinling orogen, central China. *Tectonophysics* 323, 183–196. doi:10.1016/S0040-1951(00)00106-2
- Nie, H., Yao, J., Wang, X., Zhu, X. Y., Wolfgang, S., and Chen, F. (2016). Precambrian tectonothermal evolution of South qinling and its affinity to the Yangtze block: evidence from zircon ages and Hf-Nd isotopic compositions of basement rocks. *Precambrian Res.* 286, 167–179. doi:10.1016/j.precamres.2016.10.005
- Nie, H., Ye, R. S., Cheng, H., Zhu, X. Y., and Chen, F. K. (2019). Neoproterozoic intrusions along the Northern margin of South Qinling, Central China: Geochemistry, zircon ages, and tectonic implications. *Precambrian Res.* 334, 105406. doi:10.1016/j.precamres.2019.105406
- Niu, Y., and O'Hara, M. J. (2003). Origin of ocean island basalts: A new perspective from petrology, geochemistry, and mineral physics considerations. *J. Geophys. Res.* 108 (4), 283–299. doi:10.1029/2002JB002048
- Pearce, J. A. (2008). Geochemical fingerprinting of oceanic basalts with applications to ophiolite classification and the search for Archean oceanic crust. *Lithos* 100 (1-4), 14–48. doi:10.1016/j.lithos.2007.06.016
- Qiu, X. F., Ling, W. L., Liu, X. M., Yang, H. M., Duan, R. C., and Lu, S. S. (2013). Zircon Hf isotope of Shennongjia volcanic rocks on the northern margin of the Yangtze craton. *Geol. Bull. China* 32 (9), 1394–1401. doi:10.3969/j.issn.1671-2552.2013.09.008
- Qiu, X. F., Yang, H. M., Lu, S. S., Zhang, L. G., Duan, R. C., and Du, G. M. (2016). Geochronology of the khondalite series in the kongling complex, yangtze craton and its geological implication. *Geotecton. et Metallog.* 40 (3), 563–572. doi:10.16539/j.ddgzycx.2016.03.011
- Ratschbacher, L., Hacker, B. R., Calvert, A., Webb, L. E., Crimmer, J. C., McWilliams, M. O., et al. (2003). Tectonics of the qinling (central China): Tectonostratigraphy, geochronology, and deformation history. *Tectonophysics* 366, 1–53. doi:10.1016/S0040-1951(03)00053-2
- Roser, B. P., and Korsch, R. J. (1986). Determination of tectonic setting of sandstone-mudstone suites using SiO₂ content and K₂O/Na₂O ratio. *J. Geol.* 94 (5), 635–650. doi:10.1086/629071
- Roser, B. P., and Korsch, R. J. (1988). Provenance signatures of sandstone-mudstone suites determined using discriminant function analysis of major-element data. *Chem. Geol.* 67, 119–139. doi:10.1016/0009-2541(88)90010-1
- Rudnick, R., and Gao, S. (2003). Composition of the continental crust. *Treatise geochem.* 3, 1–64. doi:10.1016/B0-08-043751-6/03016-4
- Shaw, D. M., and Kudoi, A. M. (1965). A test of the Discriminant Function in the amphibolite problem. *Mineral. Mag. J. Mineral. Soc.* 34 (268), 423–435. doi:10.1180/minmag.1965.034.268.38
- Shaw, D. M. (1972). The origin of the apsey gneiss, ontario. *Can. J. Earth Sci.* 9 (1), 18–35. doi:10.1139/e72-002
- Shen, J., Zhang, Z. Q., and Liu, D. Y. (1997). Sm-Nd, Rb-Sr, ⁴⁰Ar/³⁹Ar, ²⁰⁷Pb/²⁰⁶Pb age of the Douling metamorphic complex from Eastern Qinling orogenic belt. *Acta Geogr. Sin.* 18 (3), 248–254.
- Shi, Y., Yu, J. H., and Santosh, M. (2013). Tectonic evolution of the qinling orogenic belt, central China: New evidence from geochemical, zircon U-Pb geochronology and Hf isotopes. *Precambrian Res.* 231, 19–60. doi:10.1016/j.precamres.2013.03.001
- Simonen, A. (1953). Stratigraphy and sedimentation of the Svecofennidic, early Archean supracrustal rocks in southwestern Finland. *Bull. Comm. Geol. Finl.* 160, 1–64.
- Sun, S. S., and Macdonough, W. F. (1989). Chemical and isotopic systematics of oceanic basalts: Implications for mantle composition and processes. *Geol. Soc. Lond. Spec. Publ.* 42 (1), 313–345. doi:10.1144/GSL.SP.1989.042.01.19
- Taylor, S. R., and McLennan, S. M. (1985). *The continental crust: Its composition and evolution*. Oxford: Blackwell, 312.
- Wang, L. J., Griffin, W. L., Yu, J. H., and O'Reilly, S. Y. (2013). U-Pb and Lu-Hf isotopes in detrital zircon from neoproterozoic sedimentary rocks in the northern Yangtze block: Implications for precambrian crustal evolution. *Gondwana Res.* 23, 1261–1272. doi:10.1016/j.gr.2012.04.013
- Wang, R. M. (1987). *Graphic discrimination of metamorphic protolith*. Beijing, China: Geological Publishing House.
- Wang, Z. Q., Yan, Q. R., Yan, Z., Wang, T., Jiang, C. F., Gao, L. D., et al. (2009). New division of the main tectonic units of the Qinling orogenic belt, Central China. *J. Geol.* 3 (11), 1527–1546. doi:10.3321/j.issn:0001-57
- Wiedenbeck, M., Alle, P., Corfu, F., Griffin, W. L., Meier, M., Oberli, F., et al. (1995). Three natural zircon standards for U-Th-Pb, Lu-Hf, trace element and REE analyses. *Geostand. Geoanal. Res.* 197–218, 1–23. doi:10.1111/j.1751-908X.1995.tb00147.x
- Winchester, J. A., and Floyd, P. A. (1977). Geochemical discrimination of different magma series and their differentiation products using immobile elements. *Chem. Geol.* 20 (1), 325–343. doi:10.1016/0009-2541(77)90057-2
- Wu, Y. B., and Zheng, Y. F. (2012). Tectonic evolution of a composite collision orogen: an overview on the qinling-tongbai-hong'an-dabie-sulu orogenic belt in central China. *Gondwana Res.* 23, 1402–1428. doi:10.1016/j.gr.2012.09.007
- Wu, Y. B., Zhou, G. Y., Gao, S., Liu, X. C., Qin, Z. W., Wang, H., et al. (2014). Petrogenesis of neoproterozoic TTG rocks in the Yangtze craton and its implication for the formation of archaic TTGs. *Precambrian Res.* 254, 73–86. doi:10.1016/j.precamres.2014.08.004
- Xiao, Y. Y., Chen, S., Niu, Y. L., Wang, X. H., Xue, Q. Q., Wang, G. D., et al. (2020). Mineral compositions of syn-collisional granitoids and their implications

for the formation of juvenile continental crust and adakitic magmatism. *J. Pet.* 61, 1–19. doi:10.1093/petrology/egaa038

Yang, B. H., Zhang, C. L., and Li, L. (2011). Sr-Nd-Pb Isotopic characteristics of the granitoids in the Douling complexes, Eastern Qinling, China and its geological significance. *Geol. Bull. China*. 30 (2-3), 439–447. doi:10.3969/j.issn.1671-2552.2011.02.031

Yang, X. L., Zhu, M. Y., Zhao, Y. L., Zhang, J. M., and Guo, Q. J. (2008). Re geochemical characteristics of the Ediacaran-lower Cambrian black rock series in eastern Guizhou. *Geol. Rev.* 54 (1), 3–15. doi:10.1016/S1872-5791(08)60056-1

Yuan, H. L., Gao, S., Dai, M. N., Zong, C. L., Günther, D., Fontaine, G. H., et al. (2008). Simultaneous determinations of U-Pb age, Hf isotopes and trace element compositions of zircon by excimer laser-ablation quadrupole and multiple-collector ICP-MS. *Chem. Geol.* 247 (1-2), 100–118. doi:10.1016/j.chemgeo.2007.10.003

Zhang, G. W., Zhang, B. R., Yuan, X. C., and Xiao, Q. H. (2001). Qinling orogen belt and continental geodynamics. *Sci. Press* 729.

Zhang, H., Cheng, H., Wu, G., Huang, X., and Chen, F. (2021). Fluid-fluxed melting of orogenic crust in the south qinling belt, central China: Implications from

migmatites of the foping dome. *J. Asian Earth Sci.* 206 (5), 104606. doi:10.1016/j.jseas.2020.104606

Zhang, S., Zhang, Z., Song, B., Tang, S., and Zhao, Z. (2004). On the existence of Neoproterozoic materials in the Douling complex, Eastern Qinling-evidence from U-Pb shrimp and Sm-Nd geochronology. *Acta Geol. Sin.* 78 (6), 800–806. doi:10.3321/j.issn:0001-5717.2004.06.010

Zhang, Z. Q., Zhang, G. W., and Tang, S. H. (2002). *Isotopic chronology of South Qinling metamorphic rock-group*. Beijing: Geological Publishing House, 1–256.

Zhang, Z. Q., Zhang, G. W., Tang, S. H., and Wang, J. H. (2001). On the age of metamorphic rocks of the Yudongzi group and the Archean crystalline basement of the Qinling Orogen. *Acta Geol. Sin.* 12 (6), 739–773. doi:10.3321/j.issn:0001-5717.2001.02.008

Zhen, S. X. (2014). “Petrogenesis and tectonic significance of the marble within hongqiyinzi complex in north Hebei Province, China,” Doctoral dissertation (Chengdu: Chengdu University of Technology).

Zhu, X. Y., Chen, F. K., Li, S. Q., Yang, Y. Z., Nie, H., Siebel, W., et al. (2011). Crustal evolution of the North Qinling terrain of the Qinling Orogen, China: Evidence from detrital zircon U-Pb ages and Hf isotopic composition. *Gondwana Res.* 20, 194–204. doi:10.1016/j.gr.2010.12.009